CFIRE

Effects of Heavy Vehicles on Dynamic Traffic Features

CFIRE 09-08
February 2016

National Center for Freight & Infrastructure Research & Education
Department of Civil and Environmental Engineering
College of Engineering
University of Wisconsin–Madison

Authors:
Danjue Chen, Soohyuk Bang, Soyoung Ahn, and David Noyce
Department of Civil and Environmental Engineering, University of Wisconsin–Madison

Principal Investigators:
Soyoung Ahn
Department of Civil and Environmental Engineering
University of Wisconsin–Madison

David Noyce
Department of Civil and Environmental Engineering
University of Wisconsin–Madison

This page intentionally left blank.

Technical Report Documentation

1. Report No. CFIRE 09-08	2. Government Accession No.	3. Recipient's Catalog No. **CFDA 20.701**	
4. Title and Subtitle Effects of Heavy Vehicles on Dynamic Traffic Features		5. Report Date **February 2016** 6. Performing Organization Code	
7. Author/s Danjue Chen, Soohyuk Bang, Soyoung Ahn, David Noyce: Department of Civil and Environmental Engineering, University of Wisconsin-Madison		8. Performing Organization Report No. **CFIRE 09-08**	
9. Performing Organization Name and Address National Center for Freight and Infrastructure Research and Education (CFIRE) University of Wisconsin-Madison 1415 Engineering Drive, 2205 EH Madison, WI 53706		10. Work Unit No. (TRAIS) 11. Contract or Grant No. T002688	
12. Sponsoring Organization Name and Address US Department of Transportation The Office of the Secretary of Transportation – Research 1200 New Jersey Avenue, SE Washington, DC 20590		13. Type of Report and Period Covered **Final Report 9/1/2014–1/31/2016** 14. Sponsoring Agency Code	
15. Supplementary Notes Project completed by Department of Civil Engineering and Environmental Engineering for CFIRE.			
16. Abstract Traffic congestion on highways has been growing in urban areas where freight transportation hubs reside, affecting the efficiency and reliability of freight transportation. This research will investigate the effects of heavy vehicles on dynamic traffic patterns that substantially affect highway performance. To understand the underlying mechanisms, this research will analyze and model car-following and lane-change behavior involving heavy vehicles. These models will be used to simulate various traffic scenarios to examine the impact of heavy vehicles on bottleneck capacity drop and characteristics of stop-and-go oscillations. Potential impacts of Connected Vehicle technology for heavy vehicles will also be evaluated. Simulated vehicle trajectories will be used for obtaining travel time distributions for uncertainty assessment. The intent of this research is to help develop effective controls that can improve overall highway traffic operations while accommodating freight vehicles, an important step in improving the reliability of freight transportation.			
17. Key Words Bottlenecks; Car following; Freight traffic; Heavy vehicles; Highway operations; Lane changing; Mobile communication systems; Traffic congestion; Traffic simulation; Travel time	18. Distribution Statement **No restrictions. This report is available through the Transportation Research Information Services of the National Transportation Library.**		
19. Security Classification (of this report) **Unclassified**	20. Security Classification (of this page) **Unclassified**	21. No. of Pages 77	22. Price **-0-**

Form DOT F 1700.7 (8-72) Reproduction of form and completed page is authorized.

DISCLAIMER

This research was funded by the National Center for Freight and Infrastructure Research and Education. The contents of this report reflect the views of the authors, who are responsible for the facts and the accuracy of the information presented herein. This document is disseminated under the sponsorship of the US Department of Transportation, University Transportation Centers Program, in the interest of information exchange. The US Government assumes no liability for the contents or use thereof. The contents do not necessarily reflect the official views of the National Center for Freight and Infrastructure Research and Education, the University of Wisconsin–Madison, or the US DOT's RITA at the time of publication.

Project Summary

Traffic congestion on highways has been growing in urban areas where freight transportation hubs reside, affecting the efficiency and reliability of freight transportation. This research investigated the effects of heavy vehicles (HVs) on dynamic traffic patterns that substantially affect highway performance. Particularly, the objective of this study is two-fold: (1) to characterize the car-following (CF) and lane-change (LC) behavior involving HVs at the individual vehicle level, and (2) to quantify the effects of HVs in traffic streams in two typical types of highway bottleneck, rubbernecking and uphill segment.

This study first calibrated three well-known CF models, Newell's model, Gipps' model, and Intelligent Driver Model (IDM), using real trajectory data to examine their effectiveness in describing the behavior of HVs. It was found that the model performance, in terms of errors, varied with time resolution of data in calibration. The performance of IDM deteriorates with time resolution, but Newell's model improved as the time resolution increased. The errors of Gipps' model exhibited a convex relationship with the time resolution. IDM performed the best when the time resolution was small but as the time resolution increased, Newell's model eventually surpassed IDM. Parameters in Newell's model were found to be insensitive to the time resolution, but a large proportion of parameters in IDM and Gipps' model were very sensitive to the resolution changes, which presents a challenge for calibration. Therefore, a comprehensive evaluation of model's advantage and limitations suggested that Newell's model is advantageous because (1) the model structure is extremely simple while it produces reasonable performance, (2) the calibrated parameters are not sensitive to the time resolution used in calibration, (3) the model parameters have clear physical meaning and can be measured directly from empirical data, and (4) extended models based on Newell's model had demonstrated the capability to capture the formation and development mechanisms of stop-and-go oscillations.

For further study, the asymmetric behavioral model (AB model), an extended Newell's model, was modified to capture the CF behavior of HVs, because (1) the model parameters have clear physical meaning that could be measured directly from the empirical data, and (2) the model describes driving behavior at the individual vehicle level, which was critical to study the mechanisms of formation and development of stop-and-go oscillations and the impacts of oscillations on traffic flow, such as capacity-drop (i.e., reduction in bottleneck discharge rate). Specifically, an empirical analysis was conducted, in the framework of the AB model, to study the CF behavior of HVs and passenger cars (PCs) around HVs. Three CF combinations were examined, HV-following-PC (HV-PC), PC-following-HV (PC-HV), and PC-following-PC (PC-PC). It was found that different vehicle combination of CF pairs had very different features when experiencing stop-and-go traffic. The PC-HV case showed the largest time gap (τ) and PC-PC showed the smallest gap. More importantly, HV-PC pairs exhibited a significant dampening effect by decreasing speed variations of stop-and-go disturbances. This effect was associated with the convex or non-increasing reaction patterns of HVs in responding to stop-and-go waves, in which HVs either responded late or decelerated in a milder way. On the other hand, HVs maintained much larger spatial gap, resulting in lower flow (in veh/h).

This study also conducted an empirical analysis of LC behavior around HVs. It was found that HVs had the discouraging effect; i.e., they discouraged other vehicles to insert behind them, presumably due to less desirable CF conditions (e.g., limited sight distance). This effect favored traffic stability by reducing potential disturbance imposed by LCs, but could undermine roadway utilization by creating large gap behind HVs. For both CF and LC behavior, there were behavioral aspects that could favor and undermine the traffic flow efficiency, and the interaction was complex. A comprehensive evaluation of HVs integrating both CF and LC behavior is needed in future research.

Based on the results of empirical studies, this study conducted simulations to study the impacts of the CF behavior of HVs in two typical types of highway bottleneck: rubbernecking and uphill segment. In the

rubbernecking experiment, it was found that HVs reduced the formation and growth of traffic oscillations. This resulted in reduced overall capacity-drop: the normalized bottleneck discharge flow in PC/h increased with HV proportion. In the uphill experiment, it was found that restrained acceleration due to roadway grade could cause a significant reduction in discharge flow and that the effect was much more profound for HVs than PCs. It was also found that the effect of variable driver characteristics diminished with the grade and HV proportion. Lastly, with given positive grade, the effects of HV proportion quickly diminished and became marginal, which was a puzzling result. It is suspected that it is a result of complex interactions among grade, vehicle mechanics, and variable driver characteristics. Further studies are needed to elucidate these interactions.

Further research is also needed to obtain a more complete understanding of HVs' impact and develop control strategies based on the insight from this study. Particularly, due to the data limitation, this research was unable to build a meaningful LC model. A future study on LC modeling will facilitate integration of CF and LC models and a comprehensive evaluation of HV's impact.

Contents

1 Introduction

Efficient and reliable highway systems are critical for freight transportation to maintain economic competitiveness. Traffic congestion results in longer and more uncertain highway travel time, which is especially problematic for freight systems that need to maintain sufficient quality of service.

Two phenomena of highway traffic are particularly important for freight transportation: bottleneck "capacity drop" and stop-and-go traffic (termed oscillations). These phenomena affect travel time and its reliability, and induce higher energy use and emissions due to frequent deceleration-acceleration (particularly in oscillations). The first phenomenon refers to a reduction in bottleneck discharge flow with onset of recurrent congestion (Banks, 1991; Cassidy and Bertini, 1999). This phenomenon is prevalent near busy merges and weaves, and is attributed to systematic lane changes (LC) in near-capacity states (Elefteriadou et al., 1995; Cassidy and Rudjanakanoknad, 2005). These LC create voids in traffic streams due to bounded vehicle accelerations (Laval and Daganzo, 2006), resulting in a 5-25% reduction in bottleneck discharge flow.

The second phenomenon, stop-and-go oscillations, frequently emerges in congested traffic near bottlenecks (Ahn and Cassidy, 2007). They exhibit regularities in period (2-10 min) and propagation speed (10-15 mph) and grow significantly in amplitude as they propagate through congested traffic (Mauch and Cassidy, 2002; Ahn and Cassidy, 2007). The formation and growth of oscillations have been linked to instabilities in car-following (CF) (Zheng et al., 2011), LC (Ahn and Cassidy, 2007; Zheng et al., 2011), and driver characteristics (Laval and Leclercq, 2010; Chen et al., 2012). Notably, driver reaction patterns to oscillations can further reduce the bottleneck discharge rate (Chen et al., 2014).

Exiting literature on the behavior and impacts of heavy vehicles (HVs) is very limited. There have been some efforts to characterize the behavioral difference in CF and impact in traffic streams. The majority of the efforts, however, entailed modifying some parameters (such as space and headway) of existing CF

models originally developed for passenger cars (PCs) and examining the impact using simulation (e.g., literature in (Jo et al., 2003; Yang & Regan, 2008; Grenzeback et al., 1990; Peeta et al., 2005, Hoel & Peek, 1999)). A few recent studies used empirical vehicle trajectory data for model calibration (e.g., Ossen & Hoogendoorn, 2011, Yang et al., 2013) or to extract statistic characteristics (e.g., headway) (Aghabayk et al., 2012). These studies cited, however, applied the data in an aggregate way. This is a significant drawback because the aggregation could not reveal the driver characteristics at the individual level, which were shown to be critical in the formation and development mechanisms of stop-and-go oscillations (Chen et al., 2012a, b, Chen et al., 2014).

Literature on the LC behavior involving HVs is sparser. Existing studies have mainly focused on the involvement of HVs in LC related crashes. For example, an NHTSA report (Sen et al., 2002) examined the lane-changing crashes in 1999 in the US and found that large trucks were involved in 15% of the "typical lane changes". Particularly, large trucks were involved in 42% of the "merge" scenario crashes. Some studies on truck-lane restrictions implicitly examined this issue by comparing LC rates before and after the restrictions; however, the results were mixed (e.g., literature in (Hoel & Peek, 1999, Gan & Jo, 2003; Jasek, 1997; Cate & Urbanik, 2004; EI-Tantawy, 2009)). To our best knowledge, no empirical studies have examined the LC behavior involving HVs at the individual vehicle level.

HVs can affect the above phenomena in a number of ways. In congested traffic, HV tend to maintain larger headway and spacing for any given speed than PCs (Aghabayk et al., 2012), suggesting lower overall throughput in vehicles per hour. More importantly, due to their physical dimension and weight, HVs have more limited acceleration and deceleration capabilities. Thus, HVs may react very differently to stop-and-go oscillations and significantly change the propagation characteristics. Last but not the least, the compound impacts of HVs may vary significantly with the geometric features of roadways, such as flat road and uphill. The mechanisms of the above traffic dynamics are currently not well understood and will be explored extensively in this proposed research. Note that the current literature provides extensive knowledge of the mechanisms for PC, which will be used as a building block for this research.

Note that the purpose of this research is to better understand the dynamics of heterogeneous traffic and its impact on the highway traffic operations, which will lay the foundation for development of traffic control strategies to improve energy efficiency, environmental emission, and overall society mobility. This is particularly important for the innovative application of emerging vehicle technologies, such as connected and automated vehicle technologies, to improve the traffic operation and promote smart and green truck freight.

The remaining report is structured as follows. Chapter 2 describes the project scope and Chapter 3 provides an introduction on the background of the study, particularly on the relevant literature. Chapter 4 presents the results of model calibration involving HVs against three typical car-following models. Chapter 5 and 6 respectively induce the empirical study of the CF and LC behavior of HVs. Car-following simulations using the model obtained from Chapter 5 are presented in Chapter 7, followed by conclusions and discussion in Chapter 8.

2 Project Scope

The objective of this study is (1) to characterize the CF and LC behavior involving HVs at the individual vehicle level, and (2) to quantify the impacts of HVs in traffic streams in two typical types of highway bottleneck through simulations: rubbernecking and uphill segment. Specifically, for (1) this project examined (i) the differences in CF behavior, particularly reaction patterns to oscillations, among three cases: HV-following-PC (HV-PC), PC-following-HV (PC-HV), and PC-following-PC (PC-PC), (ii) the differences in LC rates around HVs as opposed to PCs, and (iii) the unique impact of these differences in development of oscillations, based on empirical analysis of high resolution vehicle trajectory data. With the CF model developed for HVs, this project conducted simulations to study (i) the effects of HVs' CF behavior in oscillatory traffic, particularly on bottleneck discharge flow and oscillation period and amplitude; and (ii) how the effects change with respect to the grade. The simulations provided insights into HVs' role in dampening oscillations and the interaction among HVs' vehicle characteristics, driving characteristics, and roadway grade conditions, which allowed further formulation and quantification of HVs' impacts in traffic streams and enabled further control strategies.

3 Project Background

3.1 Literature on HV Modeling

HVs presumably exhibit or induce different CF and LC behavior than PCs due to their substantially heavier weight and larger physical dimensions, which can uniquely impact the traffic stream. There have been some efforts to characterize the behavioral difference in CF and impact in traffic streams. The majority of the efforts, however, entailed modifying some parameters (such as space and headway) of existing CF models originally developed for PCs and examining the impact using simulation (e.g., literature in (Jo et al., 2003; Yang & Regan, 2008; Grenzeback et al., 1990; Peeta et al., 2005, Hoel & Peek, 1999)). More recently, several empirical studies examined CF behavior involving HVs using real vehicle trajectory data. A brief introduction of the major studies is provided below.

Ossen & Hoogendoorn (2011) used trajectories collected by helicopter to calibrate the car-following behavior of passenger car following passenger car and passenger car following trucks. They calibrated 8 car-following models to find the three best fitted models. It was found that there was significant difference: the desired time headway of passenger car drivers was smaller when they were following trucks than when they were following passenger cars.

Aghabayk et al. (2012) examined the characteristics (e.g., headway) of different CF combinations (car-following-car, car-following-truck, and truck-following-car) by aggregating the trajectory sample of each CF type. It was found that for space and time headways, truck-following truck pairs had the largest and car-following-car pairs had the smallest values. In very low speed condition (speed below 30 km/h), car-following-truck had larger space and time headway than truck-following-car pair but the relationship was reversed when speed was higher (i.e., speed larger than 30 km/h). The authors claimed that when speed was under 30 km/h, as the followers, the cars desired to secure the sight distance behind the truck to maintain large headway. By contrast, in high speed, the following trucks desired to keep large headway

out of the concern of limited braking capability. Notably, these results were different from the results of Ossen & Hoogendoorn (2011), which found that the reaction time in car-following-truck and truck-following-car pairs was the same.

Yang et al. (2013) used NGSIM trajectory data to calibrate the Intelligent Driver Model (IDM) (Treiber et al., 2000) for different CF combinations. They found that truck-following truck pairs had the largest jam space and car-following-car pairs showed the smallest jam space. Regarding the safe time headway, the value was the largest in truck-following-truck pairs, followed by car-following-truck pairs and then truck-following-car pairs, and it was the smallest in the car-following-car pairs. Notably, these results were mostly consistent with the results of of Aghabayk et al. (2012). Yang et al. (2013) also found that cars and HVs can both stabilize and destabilize traffic flow depending on the CF combination types and equilibrium velocity.

It is worth noting that the results on the CF model calibration for HVs were inconsistent in the studies introduced above. Additionally, these studies studied the HV characteristics in an aggregate way. This method, however, could cause significant problems because the studies of Chen et al. (2012a), Chen et al. (2012b) and Chen et al. (2014) revealed that the individual driver characteristic is critical to describing stop-and-go oscillation formation and development and to capturing the impacts on traffic flow such as capacity-drop.

The literature on the LC behavior involving HVs is even sparser. Existing studies have mainly focused on the involvement of HVs in LC related crashes. For example, an NHTSA report (Sen et al., 2002) examined the lane-changing crashes in 1999 in the US and found that large trucks were involved in 15% of the “typical lane changes”. Particularly, large trucks were involved in 42% of the “merge” scenario crashes. Some studies on truck-lane restrictions implicitly examined the impacts of HVs by comparing LC rates before and after the restrictions; however, the results were mixed (e.g., literature in (Hoel & Peek, 1999, Gan & Jo, 2003; Jasek, 1997; Cate & Urbanik, 2004; EI-Tantawy, 2009)). To our best

knowledge, no empirical studies have examined the LC behavior involving HVs at the individual vehicle level.

The results of literature review suggest that though HVs play an important role in the traffic stream, our understandings on the HV behavior (including CF and HV behavior) are still in the infancy. This impedes the application of emerging new technologies, such as connected and automated vehicles technologies, for further improvement. Therefore, this study aims to have better understandings of both the CF and HV behavior of HVs at the individual vehicle level, and to enable further modeling as well as control.

3.2 Existing CF models for PCs

The literature for CF behavior of PCs is very extensive. Therefore, some CF models for PCs had been adopted and modified to represent HV's CF behavior by previous research, such as Ossen & Hoogendoorn (2011) and Yang et al (2013). Particularly, we found that in the literature three typical models were commonly used, which show the best performance in terms of data fitting and physical interpretation of calibration, Newell's model (Newell, 2002), Gipps' model (Gipps, 1981), and intelligent driver model (IDM) (Treiber et al., 2000).

3.2.1.1 Newell's Model

Newell's model (Newell, 2002) is one of the simplest car-following models. It assumes that a follower's trajectory is a transplantation of the leader's by a time and space shift (τ, d) where d represents the minimum spacing and τ represents the response time; see Figure 3-1. The two variables (τ, d) remain constant for a given CF vehicle regardless of speed but vary across different vehicles. In many studies, the ratio of d and τ, which yields the wave speed ($w = d/\tau$), is assumed constant across vehicles.

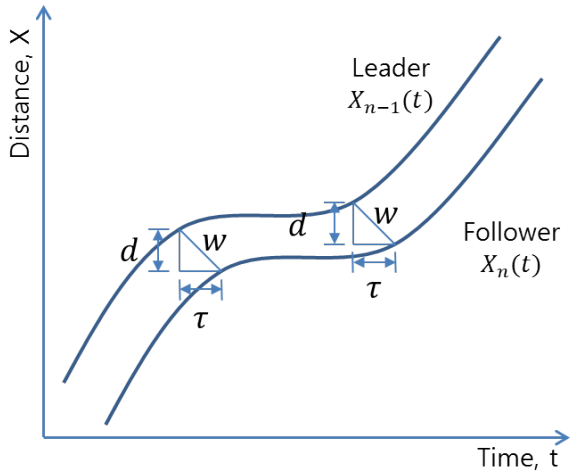

Figure 3-1: Trajectories of a vehicle pair for Newell model

Newell's model describes vehicle's position in congestion as follows:

$$X_n(t+\tau) = X_{n-1}(t) - d, \tag{1}$$

where X_n represents the position of vehicle *n*. In free-flow condition, vehicles travel at constant desired speed u.

Notice that Newell's model describes the microscopic behavior of an individual vehicle. When aggregated to the macroscopic level, the model is consistent with the Kinematic Wave model (Lighthill and Whitham, 1955; Richards, 1956) with a triangular shape fundamental diagram (as illustrated in Figure 3-2). Specifically, based on flow conservation, the Kinematic wave model describes the relationship between flow (q) and density (k) in the following form:

$$\frac{\partial k}{\partial t} + \frac{\partial q(k)}{\partial x} = 0.$$

When a triangular shape function is assigned to the flow function $q(k)$, the model becomes consistent with Newell's model.

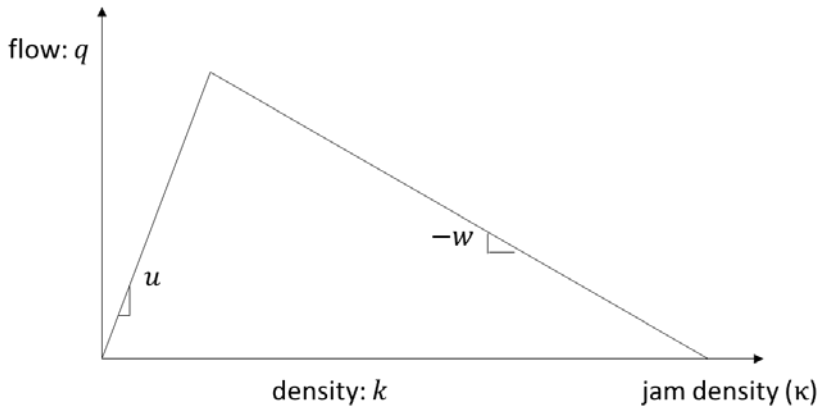

Figure 3-2: Kinematic Wave model with a triangular shape fundamental diagram

Although Newell's model has an extremely simple structure, many empirical studies suggest that the model effectively captures key traffic characteristics and provides reasonable approximations for traffic evolution. For example, Ahn et al. (2004) verified Newell's model by examining the trajectories of vehicles discharging from a long queue of a signalized intersection. They found that the time-space trajectory of a vehicle followed the vehicle in front after a time and space shift (τ, d), and there was no statistically significant difference in the (τ, d) across the observed vehicles.

3.2.1.2 Gipps' Model

Gipps' model (Gipps, 1981) adopted the safety distance logic: the speed for a given condition is derived to assure that a vehicle can safety stop in case that the proceeding vehicle suddenly decelerates. The model consists of two components: one for the free flow regime and one for the congested regime (i.e., car-following regime). In the former case, the speed of vehicle n is determined as:

$$v_{a,n}(t+\tau) = v_n(t) + 2.5 \cdot a_n^{max} \cdot \tau \cdot \left(1 - \frac{v_n(t)}{V_n^{max}}\right) \cdot \sqrt{0.025 + \frac{v_n(t)}{V_n^{max}}}. \quad (2)$$

While in the car-following regime, vehicle speed is described as:

$$v_{b,n}(t+\tau) = -b_n \cdot \left(\frac{\tau}{2} + \theta\right)$$

$$+\sqrt{b_n^2 \cdot \left(\frac{\tau}{2} + \theta\right)^2 + b_n \cdot \left[2 \cdot (x_{n-1}(t) - x_n(t) - S_{n-1}) - \tau \cdot v_n(t) + \frac{v_{n-1}(t)^2}{\hat{b_{n-1}}}\right]}. \quad (3)$$

The definitions and typical values of the variables in the model were provided in Table 2-1.

Gipps' model has been widely used in many simulation models, including the commonly used simulation software AIMSUN developed by TSS (Barcelo and Casas, 2005).

Table 2-1 Definition and typical values for parameters in Gipps' model

Notation	Meaning	Typical value (cars for urban area)
a^{max}	Maximum acceleration	2 m/s^2
τ	Apparent reaction time	1.0 sec
V^{max}	Maximum desired speed	30 m/s
b	Most severe braking	2 m/s^2
θ	Additional comfort time lag (=$\tau/2$)	0.5 sec
S	Effective vehicle size (= vehicle length + safety gap)	-
Safety gap	Gap that a following vehicle will not intrude even when vehicles stop.	2 m
$\hat{b}$	Estimate of maximum deceleration	2 m/s^2

3.2.1.3 Intelligent Driver Model (IDM)

IDM is also among the most widely used models (e.g., it was used in Ossen & Hoogendoorn, 2011; Yang et al., 2013; and Talebpour & Mahmassani, 2015). The model takes the desired speed and desired space headway into consideration and uses a single equation to capture the traffic dynamic regardless of the traffic state (i.e., congestion or free-flow). It defines the acceleration function as follows:

$$\frac{d^2 x_n(t)}{dt^2} = a \cdot \left[1 - \left(\frac{v_n(t)}{V}\right)^{\delta} - \left(\frac{S(v_n(t), \Delta v_n(t))}{\Delta x_n(t) - l}\right)^2\right], \quad (4)$$

$$S\left(v_n(t), \Delta v_n(t)\right) = s^0 + s^1 \cdot \sqrt{\frac{v_n(t)}{V}} + \tau \cdot v_n(t) - \frac{v_n(t) \cdot \Delta v_n(t)}{2 \cdot \sqrt{ab}}, \quad (5)$$

where $\Delta v_n(t) = v_{n-1}(t) - v_n(t)$, representing the difference of speed between a following vehicle and leading vehicle. The description of other variables and typical values are summarized in Table 2-2. Notice that this model would produce smooth transition from free-flow state to congestion state. The model also constrains the acceleration (deceleration) within the maximum acceleration (desired deceleration) to avoid unrealistic values. This leads to more realistic driving mechanics for the drivers. However, the model uses "desire measurements" (such as desired deceleration and desired velocity), which are difficult to observe and calibrate in measurable data in real traffic (Saifuzzaman and Zheng, 2014).

Table 2-2 Definitions and typical values for IDM parameters

Notation	Meaning	Typical value (cars)
a	Desired maximum acceleration	0.73 $\mathrm{m/s^2}$
τ	Safe time headway	1.6 sec
V	Desired velocity	120 km/h
b	Desired deceleration	1.67 $\mathrm{m/s^2}$
δ	Acceleration exponent	4
s^0	Jam distance	2 m
s^1	Jam distance	0 m

3.2.1.4 Summary

The three CF models introduced above were studied and evaluated by Punzo & Simonelli (2005) for the CF behavior of PCs. Four models (the fourth one is a stimulus-response model named MITSIM (Ahmed, 1999; Yang and Koutsopoulos, 1996)) were calibrated and validated using trajectories of a four-vehicle platoon traveling on two different types of roadway, urban and extra-urban roads. It was found that in model calibration, Newell's model, Gipps' model, and IDM model had similar performance measured by

the root mean square percentage error (RMSPe) of inter-vehicle spacing. The results were consistent with the calibration using test track data in Brockfeld et al. (2004). More importantly, Newell's model, which had the simplest model structure, had the best performance in the model validation. Particularly, in the validation process, the calibrated parameters from one dataset (corresponding to one road way type and therefore one type of traffic condition) were used to predict the trajectories in another dataset (corresponding to another road way type and therefore another type of traffic condition). Newell's model had the smallest RMSPe on average, while more sophisticated models (such as IDM) had smaller variation in their results. This result was attributed to the simplicity of Newell's model prevented the overfitting issues, which existed in other models with more complex structure. Additionally, it was found that Gipps' model had bad performance in the validation, suggesting that the model was too sensitive to traffic conditions.

As revealed by previous studies that assessed the performance of the CF models, the three models, Newell's model, Gipps' model, and IDM, have their own advantages and disadvantages. Therefore, we believe that it is necessary to conduct model calibration for HVs, and the results are presented in the next chapter.

4 Calibration of Selected CF Models

In this section, we conduct model calibration for HVs against the three commonly used models in the literature: Newell's model, Gipps' model, and IDM.

4.1 Data

For the whole study, the NGSIM trajectory data from I 80 (NGSIM, 2006) were used. Figure 4-1(a) provides the map and sketch of the site. Vehicle trajectories were collected for 45 minutes in total over a roadway sketch of 1650ft with the resolution of 0.1 s. Traffic on this segment was heavily congested

during the study period with frequent stop-and-go waves. The vehicle speed mostly varied from 0-35 ft/s; see Figure 4-1(b) for the vehicle trajectories in the first 15 minutes of the data on lane 3. The trajectories in the figure are colored according to the speed scale shown on the right.

This study focused on three types of CF combinations: HV-PC, PC-HV, and PC-PC. The case of heavy vehicle following heavy vehicle (HV-HV) was excluded due to the small sample size. The case of PC-PC was analyzed to generate benchmark against the behavior of the other two cases. We defined HV as a vehicle (excluding buses) with length greater than 50 ft and PC as a vehicle with length smaller than 16 ft (but excluding motorcycles). For CF calibration, the dataset was further filtered to assure that the trajectory pairs were free of lane-changing impact and displayed deceleration-acceleration dynamics with speed variation greater than 10 ft/s. A total of 19, 19, and 30 CF pairs were identified for PC-HV, HV-PC, and PC-PC types, respectively.

(a)

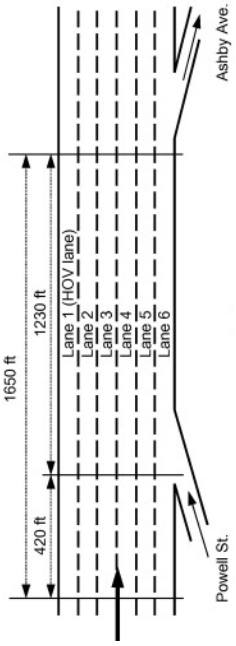

(b)

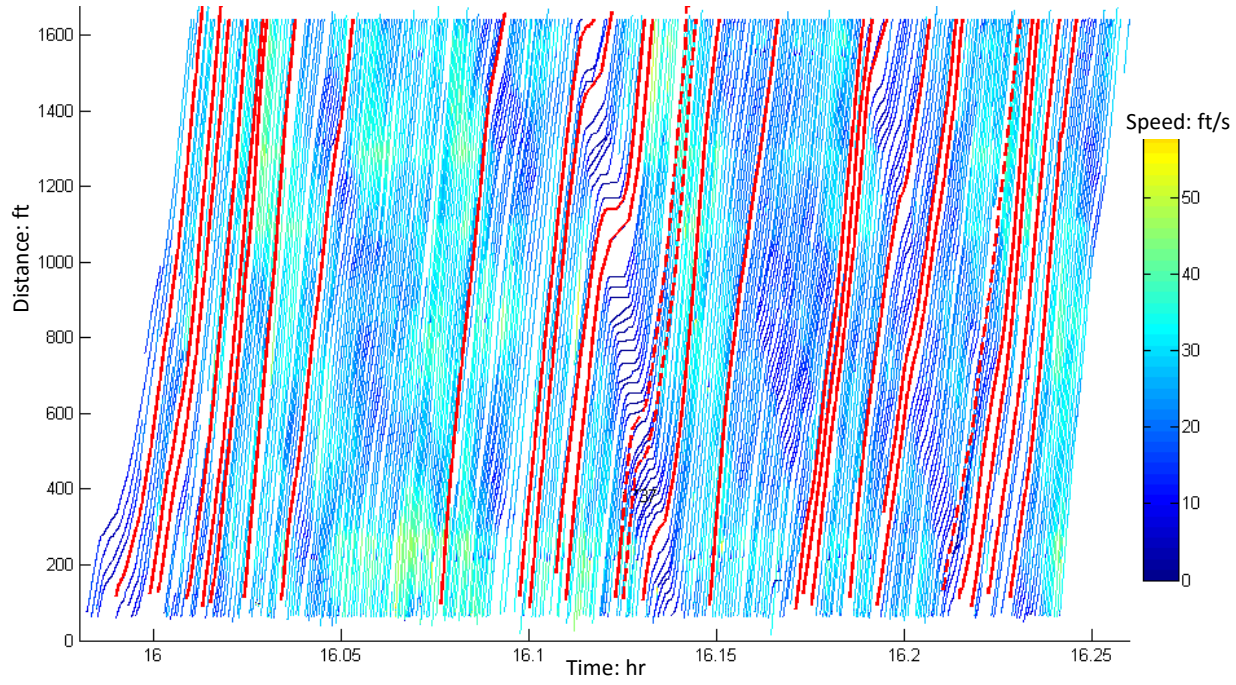

Figure 4-1: (a) Map and sketch of I 80 (Source: Google map, accessed Sep 8th, 2015); (b) Trajectory plot of I 80 lane 3 (Red trajectories are HVs).

4.2 Calibration Process

4.2.1 Genetic Algorithm

Genetic algorithm (GA) is one of the most popular optimization algorithms used for calibrating model parameters. It uses the similar method of natural selection and natural genetic (Goldberg, 1989). The major procedure of GA consists of initial generation and repeated crossover-mutation-evaluation for next generation as illustrated in Figure 4-2. Particularly, in the initial step, as the 1st generation, the algorithm generates a given number (usually a default value of 10,000) of parameter sets (each set consists of all the parameters to optimize, and the value for each parameter is randomly selected from its reasonable range). The performance of a parameter set is assessed by an objective function (described in the following subsection) that represents the error in the measurement of effectiveness (e.g., inter-vehicle spacing)

between the predicted value from the model and the real value, denoted by the score. Thereafter, the performance is used to rank the parameter sets.

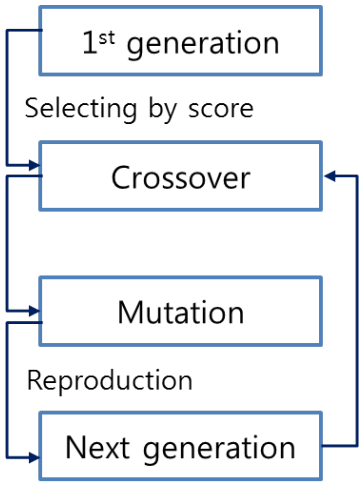

Figure 4-2: Process of Genetic algorithm

From the result of the 1st generation, a certain number of parameter sets (we use 4000 sets) are selected for crossover and mutation to further derive the optimal parameter values. In selecting parameter sets, those that are well-ranked (i.e., with higher scores) have higher probabilities (we used the default probability assignment function in Matlab's GA algorithm). With the selected parameter sets, the crossover process is applied. The underlying mechanism is to take two mutually exclusive parts of the parameter values from two different well-performed parameter sets to construct a new set of parameter values. This process is illustrated in Figure 4-3. In general, the performance of the new value set will be closer to the optimum. Following the crossover, mutation is used to assure that the optimum selected for that generation is global optimum; shown in Figure 4-4. Specifically, for a given parameter set, one parameter value is replaced with a random value, which generates a new parameter set. All the new parameter sets resulting from crossover and mutation will be used in the next generation for evaluation. The process of crossover-mutation-evaluation for next generation is repeated until the optimal values for the parameter set converge.

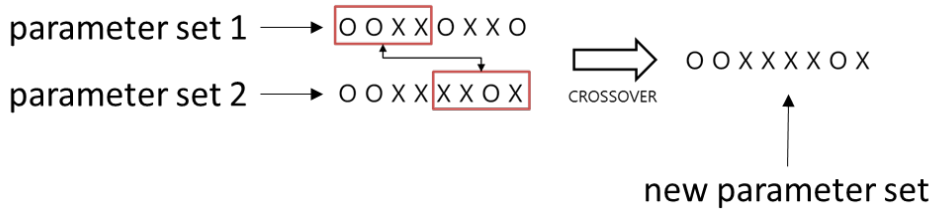

Figure 4-3: Crossover of GA for an example of 8 parameters

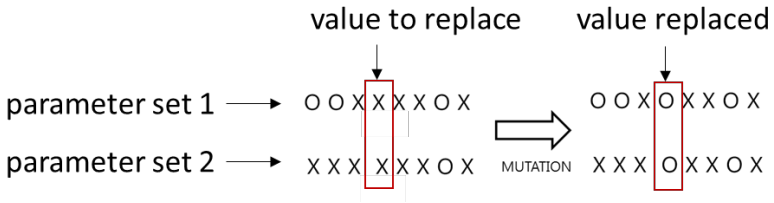

Figure 4-4: Mutation of GA (O and X denote possible outcomes of a variable)

To run GA, Matlab and global optimization toolbox were used. Note that the upper bound (UB) and lower bound (LB) for each parameter are specified as inputs to account for possible constraints. For this, we consider the physical capability of vehicles and typical values that accord well with real traffic. For example, in Newell's model the range of τ was decided by considering the distribution of driver reaction time. Reaction time less than 0.5 sec is highly unlikely for normal drivers (except for professional race drivers), and if reaction time is greater than the maximum value, it is likely that the driver is not in car-following mode. The minimum spacing, d, in Newell's model was set by considering vehicle length, which should be greater than the average length of paired vehicles. The UB and LB for parameters in Gipps' model and the IDM model were set in a similar way. Specifically, the range of desired velocity V (called maximum desired speed in Gipps's model) was set by considering the characteristics of cars and trucks and the speed limit of the study segment. Table *4-1* shows the range of parameters for the three models considered. Note that for Gipps' model, only the second equation for the car-following regime was used for the calibration because the traffic condition on I 80 was congested.

Table 4-1: (a) Parameter range of Newell's model; (b) Parameter range of Gipps' model; (c) Parameter range of IDM

(a)

Newell's model			
Parameter		LB	UB
τ (sec)		0.5	10
d (ft)	PC-PC	20	100
	PC-HV/HV-PC	40	100

(b)

Gipps' model		
Parameter	LB	UB
τ (sec)	0.5	10
b (ft/s^2)	0.1	27
Safety gap (ft)	1	33
$b\hat{}$ (ft/s^2)	0.1	27

(c)

IDM		
Parameter	LB	UB
a (ft/s^2)	0.1	8
τ (sec)	0.5	10
V (ft/s)	40	140
b (ft/s^2)	0.1	15
s^0 (ft)	0	10
s^1 (ft)	0	5

4.2.2 Objective Function

As mentioned in the previous section, to evaluate the performance of a given parameter set, an objective function is used. Here we use an objective function that aims to minimize the error between real values and estimated values from a model. Particularly, Theil's inequality coefficient *U* is adopted because it is known to produce stable and reasonable results (Yang et al., 2013).

$$U_{objective} = \frac{\sqrt{\frac{1}{K}\sum_{k=1}^{K}\left(y_k^{real} - y_k^{cal}\right)^2}}{\sqrt{\frac{1}{K}\sum_{k=1}^{K}\left(y_k^{real}\right)^2} + \sqrt{\frac{1}{K}\sum_{k=1}^{K}\left(y_k^{cal}\right)^2}}, \quad (6)$$

where y_k^{real} is the real data, y_k^{cal} is the calculated value from the model, and K is the size of the sample.

It is worth noting that the optimal parameters obtained from different runs of the GA algorithm could be slightly different because the parameter sets generated in the initial step are random. Fortunately, it is found that the optimal parameters usually converge after three runs. Therefore, for each model, GA was repeated 3 times and we chose the parameter set that led to the smallest *U* value.

4.2.3 Parameter Fitting

In parameter fitting, we first define the measurement of effectiveness. Specifically, we use the absolute Root Mean Square Error (RMSE) (defined below) and the relative error (defined as the ratio of RMSE and the average of parameter value).

$$RMSE = \sqrt{\frac{1}{K}\sum_{k=1}^{K}\left(y_k^{real} - y_k^{cal}\right)^2}. \quad (7)$$

Table 4-2 shows the results of parameter fitting for the three models with the time stamp of 0.1 s. As indicated by the table, in Newell's model the PC-PC case has the shortest reaction time, followed by the PC-HV case and then HV-PC case. Additionally, PC-PC has the smallest d and PC-HV has the largest d. In IDM, the safe time headways for PC-PC and PC-HV are similar but the value is much larger for HV-PC. Additionally, the maximum acceleration (a) for PC-PC is the largest while the values for PC-HV and HV-PC are relatively close. For Gipps' model, the reaction times for PC-PC and PC-HV are close but the value is much large for the HV-PC case. Notice that the three models do not share the same definitions for the parameters. Therefore, it is difficult to evaluate model performance based on the values of each parameter. Instead, we use speed as an indicator to assess model performance. Notice that the three

models define the car-following relationship in different forms (e.g., Newell's model describes position; Gipps' model defines speed; and IDM defines acceleration). Thus, the speed is calculated from the derivative of position in the Newell's model and from the integral of acceleration from IDM. One can see that in the relative error scale, IDM performed best with only 2% relative error in speed for all three pair combinations, and the performance of Newell's and Gipps' models was reasonably close (about 15-20%). Also note that the performance of Newell's model and Gipps' model was very similar to the result in Punzo and Simonelli (2005).

It is worth noting that the model performance varies with the resolution of the time stamp. We examined the model performance under different resolutions (0.1s, 0.5s, 1s, 2s, and 5s). The results are provided in Table 4-3, Table 4-4, and Table 4-5, and plots of model errors are provided in Figure 4-5. Clearly, the relative error in Newell's model decreases with the time resolution and becomes relatively stable after time resolution of 1s. By contrast, the relative error of IDM increases with the time resolution, which exhibits a near linear relationship. For Gipps' model, the relationship seems convex. Notably, with the time resolution of 2s, the relative errors of the three models become comparable (around 7-11%), and the performance of Newell's model eventually suppresses IDM as the time resolution continues to increase. Additionally, the model parameters show different sensitivity levels to the time resolution. Particularly, the parameter values in Newell's model seem insensitive to the time resolution increases. For example, the reaction time τ for HV-PC changes from 1.86s to 1.7s as the time resolution goes from 0.1s to 2s, with a relative scale of 8.6%. However, for IDM, a large proportion of the parameters are sensitive to the time resolution, such as maximum acceleration rate a, desired speed V, and desired deceleration rate b. For example, the desired deceleration rate b for PC-PC reduces by 31% as the time resolution goes from 0.1s to 2s. The parameters in Gipps' model are also very sensitive to the time resolution, particularly reaction time τ, most severe braking b_n, and maximum deceleration $\hat{b_{n-1}}$. Notably, the parameters in CF models are supposed to be independent of the time resolution as they should only reflect features of vehicles' driving behavior. The sensitivity to the time resolution makes the calibration process difficult because one

has to select the “correct” resolution to obtain reasonable results. Therefore, Newell’s model turns out to be advantageous with the “time resolution-independent” feature.

In model evaluation, the physical meaning of the model parameters is another important aspect. From this perspective, IDM has some limitations, though it has the minimum error level. Particularly, some key parameters in the model do not have clear physical meaning, and they are very difficult to calibrate using empirical data, such as the safe time gap (τ), which is different from reaction time, and the acceleration exponent (δ). Additionally, since the calibrated values vary with time resolution, the lack of connection to physical meaning makes it difficult to decide whether the calibrated value is reasonable or not.

Table 4-2: Calibrated parameters (time stamp=0.1 s): (a) Newell's model; (b) Gipps' model; (c) IDM

(a)

Case	τ (sec)	d (ft)	Wave speed (ft/s)	Average speed (ft/s)	RMSE (ft/s)	Relative Error
PC-PC	1.22	25.38	20.87	16.55	2.75	18%
PC-HV	1.67	68.44	40.91	14.05	2.40	19%
HV-PC	1.86	46.15	24.83	16.33	3.45	23%

(b)

Case	τ (sec)	Safety gap (ft)	b_n (ft/s^2)	$\hat{b_{n-1}}$ (ft/s^2)	Average speed (ft/s)	RMSE (ft/s)	Relative Error
PC-PC	1.45	4.34	3.64	3.50	16.55	2.31	15%
PC-HV	1.38	9.38	1.18	1.36	14.05	2.21	17%
HV-PC	1.89	5.66	2.10	3.27	16.33	2.75	18%

(c)

Case	τ (sec)	a (ft/s^2)	V (ft/s)	b (ft/s^2)	s^0 (ft)	s^1 (ft)	Average speed (ft/s)	RMSE (ft/s)	Relative Error
PC-PC	1.00	1.45	95.60	11.97	6.80	2.33	16.55	0.34	2%
PC-HV	1.10	0.50	86.25	11.36	5.15	1.17	14.05	0.25	2%
HV-PC	2.37	0.74	74.41	8.74	6.22	1.98	16.33	0.29	2%

Table 4-3: Calibrated parameters for Newell's model: (a) Time step = 0.1 s; (b) Time step = 0.5 s; (c) Time step = 1 s; (d) Time step = 2 s; (e) Time step = 5 s.

(a)

Case	τ (sec)	d (ft)	Wave speed (ft/s)	Average speed (ft/s)	RMSE (ft/s)	Relative Error
PC-PC	1.22	25.38	20.87	16.55	2.75	18%
PC-HV	1.67	68.44	40.91	14.05	2.40	19%
HV-PC	1.86	46.15	24.83	16.33	3.45	23%

(b)

Case	τ (sec)	d (ft)	Wave speed (ft/s)	Average speed (ft/s)	RMSE (ft/s)	Relative Error
PC-PC	1.30	25.55	19.62	16.35	1.65	11%
PC-HV	1.72	68.85	40.11	14.09	1.58	12%
HV-PC	1.94	46.82	24.16	16.27	2.54	17%

(c)

Case	τ (sec)	d (ft)	Wave speed (ft/s)	Average speed (ft/s)	RMSE (ft/s)	Relative Error
PC-PC	1.09	26.62	24.48	16.47	1.27	8%
PC-HV	1.97	64.85	32.84	14.15	1.27	10%
HV-PC	1.87	45.65	24.47	16.39	2.02	13%

(d)

Case	τ (sec)	d (ft)	Wave speed (ft/s)	Average speed (ft/s)	RMSE (ft/s)	Relative Error
PC-PC	1.05	36.95	35.26	16.81	1.21	8%
PC-HV	1.97	67.74	34.39	14.28	1.05	8%
HV-PC	1.70	51.86	30.42	16.66	1.72	11%

(e)

Case	τ (sec)	d (ft)	Wave speed (ft/s)	Average speed (ft/s)	RMSE (ft/s)	Relative Error
PC-PC	1.56	47.22	30.27	17.59	1.01	6%
PC-HV	2.18	84.88	38.87	14.89	0.84	6%
HV-PC	2.19	67.81	30.96	17.60	1.64	10%

Table 4-4: Calibrated parameters for Gipps' model: (a) Time step = 0.1 s; (b) Time step = 0.5 s; (c) Time step = 1 s; (d) Time step = 2 s; (e) Time step = 5 s.

(a)

Case	τ (sec)	Safety gap (ft)	b_n (ft/s^2)	$\hat{b_{n-1}}$ (ft/s^2)	Average speed (ft/s)	RMSE (ft/s)	Relative Error
PC-PC	1.45	4.34	3.64	3.50	16.55	2.31	15%
PC-HV	1.38	9.38	1.18	1.36	14.05	2.21	17%
HV-PC	1.89	5.66	2.10	3.27	16.33	2.75	18%

(b)

Case	τ (sec)	Safety gap (ft)	b_n (ft/s^2)	$\hat{b_{n-1}}$ (ft/s^2)	Average speed (ft/s)	RMSE (ft/s)	Relative Error
PC-PC	4.02	5.35	2.98	1.64	16.35	1.74	12%
PC-HV	4.52	10.08	1.31	1.08	14.09	1.65	13%
HV-PC	4.82	4.70	2.47	2.16	16.27	2.40	17%

(c)

Case	τ (sec)	Safety gap (ft)	b_n (ft/s^2)	$\hat{b_{n-1}}$ (ft/s^2)	Average speed (ft/s)	RMSE (ft/s)	Relative Error
PC-PC	4.27	5.42	2.30	1.50	16.47	1.38	9%
PC-HV	3.94	8.00	1.05	1.56	14.15	1.42	11%
HV-PC	6.01	6.51	2.10	2.72	16.39	1.91	13%

(d)

Case	τ (sec)	Safety gap (ft)	b_n (ft/s^2)	$\hat{b_{n-1}}$ (ft/s^2)	Average speed (ft/s)	RMSE (ft/s)	Relative Error
PC-PC	5.79	4.45	2.08	1.50	16.81	1.29	8%
PC-HV	3.77	7.64	1.28	1.10	14.28	1.39	11%
HV-PC	5.32	9.53	3.90	2.16	16.66	1.57	11%

(e)

Case	τ (sec)	Safety gap (ft)	b_n (ft/s^2)	$\hat{b_{n-1}}$ (ft/s^2)	Average speed (ft/s)	RMSE (ft/s)	Relative Error
PC-PC	4.30	15.43	1.69	1.93	17.59	1.80	10%
PC-HV	2.60	11.91	2.19	1.24	14.89	1.78	13%
HV-PC	4.44	17.97	4.14	1.94	17.60	1.99	12%

Table 4-5: Calibrated parameters for IDM: (a) Time step = 0.1 s; (b) Time step = 0.5 s; (c) Time step = 1 s; (d) Time step = 2 s; (e) Time step = 5 s.

(a)

Case	τ (sec)	a (ft/s^2)	V (ft/s)	b (ft/s^2)	s^0 (ft)	s^1 (ft)	Average speed (ft/s)	RMSE (ft/s)	Relative Error
PC-PC	1.00	1.45	95.60	11.97	6.80	2.33	16.55	0.34	2%
PC-HV	1.10	0.50	86.25	11.36	5.15	1.17	14.05	0.25	2%
HV-PC	2.37	0.74	74.41	8.74	6.22	1.98	16.33	0.29	2%

(b)

Case	τ (sec)	a (ft/s^2)	V (ft/s)	b (ft/s^2)	s^0 (ft)	s^1 (ft)	Average speed (ft/s)	RMSE (ft/s)	Relative Error
PC-PC	1.07	1.17	94.18	8.31	7.29	2.26	16.35	0.54	4%
PC-HV	1.21	0.46	85.61	9.10	3.95	1.83	14.09	0.47	4%
HV-PC	2.45	0.62	81.14	4.74	6.02	2.05	16.27	0.54	4%

(c)

Case	τ (sec)	a (ft/s^2)	V (ft/s)	b (ft/s^2)	s^0 (ft)	s^1 (ft)	Average speed (ft/s)	RMSE (ft/s)	Relative Error
PC-PC	1.15	1.12	82.08	7.68	7.26	2.09	16.47	0.74	5%
PC-HV	1.12	0.40	82.28	8.22	3.90	1.54	14.15	0.64	5%
HV-PC	2.46	0.54	86.83	2.94	5.63	2.37	16.39	0.71	5%

(d)

Case	τ (sec)	a (ft/s^2)	V (ft/s)	b (ft/s^2)	s^0 (ft)	s^1 (ft)	Average speed (ft/s)	RMSE (ft/s)	Relative Error
PC-PC	1.18	1.05	84.89	8.25	6.19	1.68	16.81	0.99	7%
PC-HV	1.31	0.34	85.57	7.54	2.56	0.92	14.28	0.99	7%
HV-PC	2.54	0.60	90.18	3.81	5.95	2.23	16.66	1.00	7%

(e)

Case	τ (sec)	a (ft/s^2)	V (ft/s)	b (ft/s^2)	s^0 (ft)	s^1 (ft)	Average speed (ft/s)	RMSE (ft/s)	Relative Error
PC-PC	1.15	0.73	84.91	9.59	3.71	1.44	17.59	2.17	13%
PC-HV	1.10	0.29	72.15	10.61	2.86	1.16	14.89	2.25	15%
HV-PC	3.00	1.06	73.37	7.79	2.93	1.71	17.60	1.64	10%

(a)

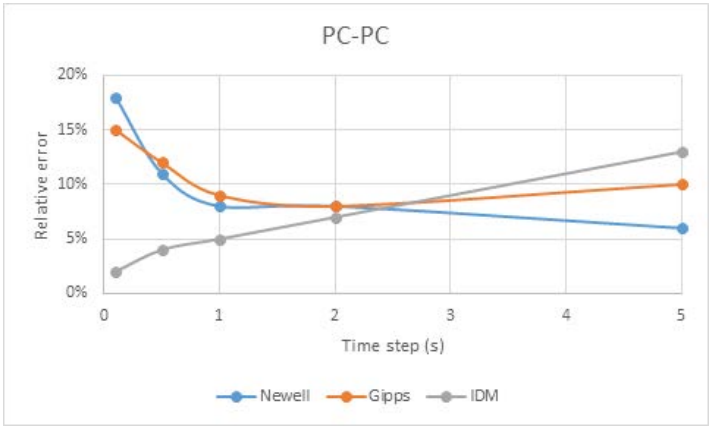

(b)

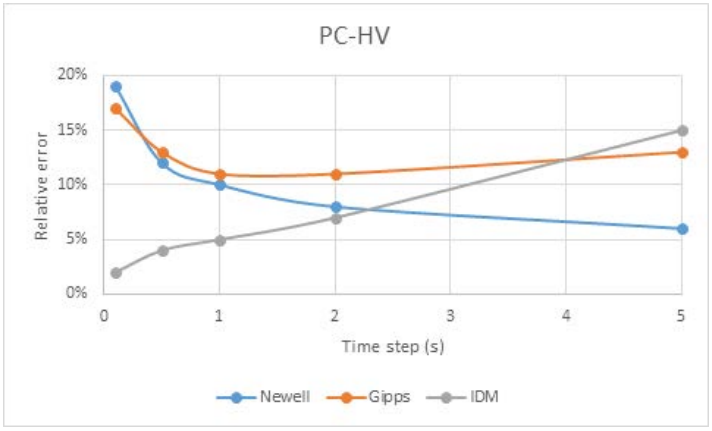

(c)

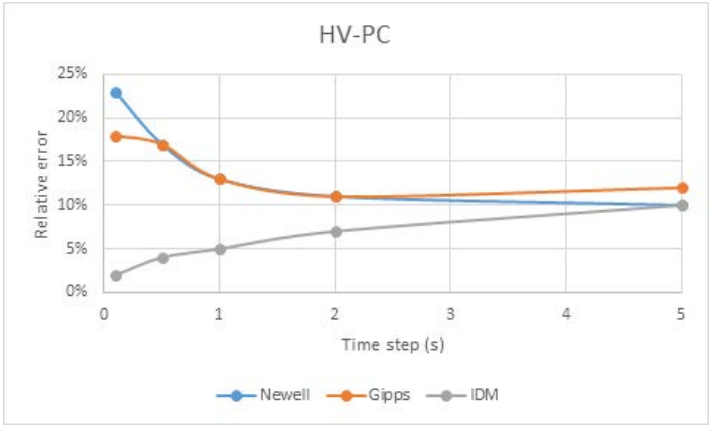

Figure 4-5: Errors vs. time resolution for (a) PC-PC case; (b) PC-HV case; (C) HV-PC case.

4.3 Summary

In this section, we calibrated the three typical CF models that are widely used in the literature, Newell's model, Gipps' model, and IDM, using the empirical vehicle trajectory data. Calibration results suggest that (1) the model performance, in terms of errors, varies with time resolution of data in calibration. The performance of IDM deteriorated with time resolution (i.e., the errors increased), but Newell's model improved as the time resolution increases. Gipps' model seems complex, with the errors showing a convex relationship with the time resolution. With the time resolution of 1s, a typical magnitude used in practice, IDM had smaller errors than Newell's model and Gipps' model (but errors for the latter two wre similar), but Newell's model eventually surpassed IDM as the time resolution continued to increase. Our analysis also suggests that (2) model parameters show different sensitivity levels to the time resolution. Newell's model was insensitive to the time resolution, and the calibrated parameter values remained stable across different resolution levels, which is a desired property for CF models. However, a large proportion of parameters in IDM and Gipps' model varied significantly as the resolution changed, which presents a challenge for calibration.

After a comprehensive evaluation of model's advantage and limitations, Newell's model turned out to be advantageous because (1) the model structure is extremely simple while it produces reasonable performance, (2) the calibrated parameters are not sensitive to the time resolution used in calibration, (3) the model parameters have clear physical meaning and can be measured directly from empirical data, and (4) extended models based on Newell's model (Laval and Leclercq, 2010; Chen et al., 2012a) have demonstrated the capability to capture the formation and development mechanisms of stop-and-go oscillations. Notice that the extended models will also lead to better model performance in terms of errors due to the more sophisticated model structure.

In the next section, we will use Newell's model and its extended models as the basic framework to revise and build a model for CF behavior of HVs.

5 Behavioral CF Model for Heavy Vehicles

5.1 Background

Chen et al. (2012a) proposed a behavioral model to capture the CF behavior of PCs at the individual level, named asymmetric behavioral model (AB model). The model is an extension of the models by Laval & Leclercq (2010) and Newell (2002). The AB model describes the time-varying CF characteristics of a vehicle when experiencing stop-and-go oscillations, given by the following equation:

$$x_{i+1}(t) = min\{x_{i+1}(t-\tau) + min\{u\tau, \tilde{x}_{i+1}(t)\},\ x_i(t-\eta_{i+1}(t)\tau) - \eta_{i+1}(t)\delta\}, \quad (7)$$

where $\tau = 1/\kappa w$ denoting the wave trip time and $\delta = 1/\kappa$ is the jam spacing in the context of the Kinematic wave model (Richards, 1956; Lighthill & Whitham, 1955) with a triangular shaped fundamental diagram. $\tilde{x}_{i+1}(t)$ is the distance that a vehicle could travel when considering bounded acceleration rate, and u is the free-flow speed. More importantly, $\eta_{i+1}(t)$, defined as the ratio of actual spacing $s_{i+1}(t)$ and equilibrium spacing $S(v_i(t_i^*))$, denotes a driver's characteristics, which captures the (time-dependent) deviation from Newell's model (Newell, 2002).

The actual and equilibrium spacing can be obtained in the following way (illustrated in Figure 5-1(a)): at a given time t on the follower's trajectory $x_{i+1}(t)$, a characteristic line with slope equal to the wave speed w is launched to intersect the leader's trajectory at time t_i^*. Then the inter-vehicle spacing assuming that the leader travels at constant speed $v_i(t_i^*)$ is the actual spacing $s_{i+1}(t)$. While the equilibrium spacing is given according to Newell's CF model (Newell, 2002) for given speed $v_i(t_i^*)$:

$$S(v_i(t_i^*)) = \delta + \tau v_i(t_i^*). \quad (8)$$

Due to the geometric similarity, the ratio of $s_{i+1}(t)$ and $S(v_i(t_i^*))$ is equivalent to the ratio of actual wave trip time $\tau_{i+1}(t)$ and the equilibrium wave trip time τ; i.e., $\eta_{i+1}(t) = \tau_{i+1}(t)/\tau$. With this relationship, the measurement of $\eta_{i+1}(t)$ boils down to measuring $\tau_{i+1}(t)$, which is much simpler: it equals to the difference between time t and time t_i^*, as illustrated in the figure. The equilibrium trip time τ, representing the average behavior of vehicles, was set to be the mean of $\tau_{i+1}(t)$ across all vehicles in steady traffic conditions.

Chen et al. (2012a,b) conducted an empirical measurement of the AB model for PCs and found that the evolution of $\eta_{i+1}(t)$ remained relatively stable before and after oscillations, denoted by η_{i+1}^0 and η_{i+1}^1 respectively, but displayed different reaction patterns during oscillations. Based on the stable level of $\eta_{i+1}(t)$ prior to the oscillation (i.e., η_{i+1}^0), drivers were categorized into three types: originally aggressive (OA) with $\eta_{i+1}^0 < 0.85$, originally timid (OT) with $\eta_{i+1}^0 > 1.15$, and originally Newell (ON) with $0.85 < \eta_{i+1}^0 < 1.15$. Also, based on the shape of $\eta_{i+1}(t)$ evolution during oscillations, four reaction patterns were identified: concave, convex, constant, and non-decreasing, as illustrated in Figure 5-1(b) below. The four patterns were approximated as triangles, with the vertex denoted by η_{i+1}^T, and the slopes of the edges denoted by ε_{i+1}^0 and ε_{i+1}^1. Thus, a driver's CF behavior can be fully described by the driver category and the reaction pattern with five parameters (η_{i+1}^0, η_{i+1}^T, η_{i+1}^1, ε_{i+1}^0, ε_{i+1}^1).

Chen et al. (2014) proposed to divide the evolution of an oscillation cycle into 4 states: precursor, growth, stable, and decay. It was found that each driver category had its preferred reaction pattern(s) and such preference varied with the development stage of the oscillation cycles. This behavioral feature of vehicles led to the formation and development of traffic oscillations. In general, OA drivers mostly adopted concave and non-decreasing reaction patterns, and OT drivers tended to use the convex pattern. While ON drivers exhibited no significant difference in using each of the four patterns. In the precursor and growth stages of oscillations, however, OA drivers had a higher probability of exhibiting the non-decreasing reaction pattern by either adopting later response to the deceleration wave or larger minimum

spacing. Consequently, these drivers exhibited $\eta_{i+1}^{1} > \eta_{i+1}^{0}$. Such behavior contributed to the significant growth in oscillation amplitude. Additionally, it can lead to reduction in discharge flow around a bottleneck; i.e., causing capacity-drop, which was confirmed by simulations.

The series of studies cited above suggest that variable driver characteristics at the individual level are critical in capturing the dynamics of oscillatory traffic. Therefore, in the following sections, we applied the framework of AB model to study the behavior of HVs.

(a) (b)

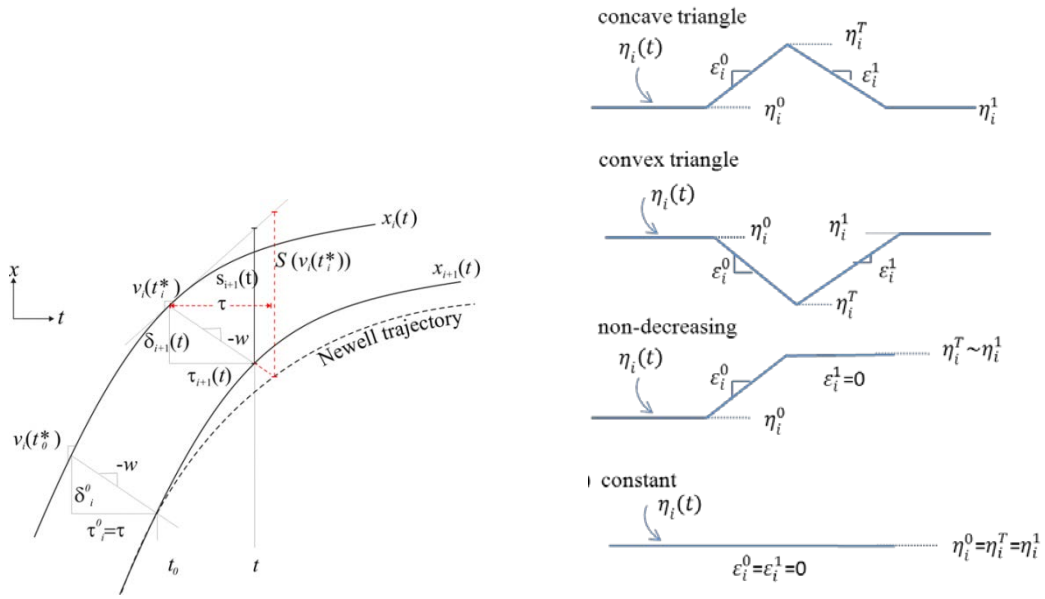

Figure 5-1 (a) Measure of $\tau_{i+1}(t)$ (Figure 4 in Chen et al. (2012a)); (b) Reaction patterns (modified based on Figure 3 in Chen et al. (2012a)).

5.2 Methodology

To study the CF behavior involving HVs, we used the same data sample as in the calibration in Chapter 4 (see the detailed introduction in Section 4.1). As introduced, this study examined three types of CF combinations: HV-PC, PC-HV, and PC-PC. The case of PC-PC is analyzed to verify that our method is

reasonable; i.e., it produces the estimates of τ, δ and w that are consistent with the values from existing studies. This case also serves as a benchmark against the behavior of the other two cases.

We analyzed the CF behavior of the three CF types by adopting the AB model. To measure the model parameters, the setting of wave speed is important as it will affect other parameters. We obtained the wave speed for each CF type by first measuring the wave speeds for individual CF pairs using the method in Chiabaut et al. (2010) and taking the average across the sample within each CF type. (The average wave speeds obtained in the fashion were also verified by the estimates from the Genetic algorithm (Goldberg, 1989) and the least square fitting for consistency.) Then, the average wave speeds were used to measure $\eta_{i+1}(t)$ for individual CF pairs.

The method in Chiabaut et al. (2010) essentially builds on Newell's car-following concept that a vehicle maintains constant (τ, δ) within the vehicle independent of speed. This method identifies the wave speed that minimizes the variation of τ expressed by the following equation:

$$s(w) = \frac{\sqrt{\frac{1}{n}\sum_{i=1}^{n}\left(\vec{w}_{|x}(\bar{u}_i,w)-\overline{\vec{w}_{|x}(\bar{u}_\iota,w)}\right)^2}}{\vec{w}_{|x}(\bar{u}_i,w)}, \quad (9)$$

where w is the wave speed value used, $\vec{w}_{|x}(\bar{u}_i, w)$ is the τ value identified for time step i, and $\overline{\vec{v}_{|x}(\bar{u}_\iota, w)}$ is the mean of $\vec{w}_{|x}(\bar{u}_i, w)$ for all time steps. The w value that minimize $s(w)$ is the optimal wave speed identified.

5.3 Results

Table 5-1 presents the optimal wave speeds identified for the three CF types and average τ and δ measured based on the optimal wave speeds. The estimated values for PC-PC are consistent with the values reported from other studies (e.g., Laval & Leclercq, 2010; Duret et al., 2011), confirming that the method is reasonable. For the case of HV-PC, both τ and δ are much greater than those for PC-PC

despite similar w values. This result is expected in view of limited acceleration/deceleration capability and much greater vehicle lengths of HVs. The case of PC-HV presents a more interesting result. The estimated τ (= 2.89 s) is the greatest of all the cases, and the estimated w is much lower (in magnitude) than the other two cases. The result suggests that when a PC is following a HV, it exhibits more 'cautious' behavior by maintaining larger time and space gaps, which could be attributable to limited sight. The result is qualitatively consistent with Aghabayk et al. (2012).

Table 5-1 CF Characteristics of CF pairs

	HV-PC	PC-HV	PC-PC
τ: s	2.1	2.9	1.2
δ: ft	44.7	37.6	27.8
w^*: ft/s	-21	-13	-23

* The negative sign denotes backward-moving waves in space.

We also examined the composition of driver category and the reaction patterns for the three CF types; see Figure 5-2 for the result. Notably, the driving behavior (i.e., relationship between driver category and reaction pattern) varies across the different CF types. Particularly, for the HV-PC case, regardless of the driver category, drivers mainly adopted convex or non-increasing reaction patterns, in which τ increases (momentarily). For the PC-HV case, the concave reaction pattern, where τ decreases momentarily, dominates in all driver categories. These features are very different from the PC-PC case, where each driver category has its preference on reaction pattern as consistent with Chen et al. (2012a) (e.g., ON drivers have an equal chance for the different reaction patterns, but OT drivers prefer convex and non-increasing patterns). Closer examination of the driving behavior of the HV-PC pairs showed that most HVs either did not respond to the deceleration of the leader immediately, or they did not decelerate as much, which led to convex or even non-increasing reaction patterns (the latter happened when a HV did not pick up speed timely during and after acceleration). This is not surprising given their limited acceleration/deceleration capability. In contrast, the analysis of the driving behavior of the PC-HV pairs revealed that when a PC perceived deceleration from the HV ahead, it tended to decelerate more (than the

leader) and then gradually speed up during acceleration, leading to the concave reaction pattern. This result, together with the larger τ and δ, suggests cautious behavior of PCs when following HVs. The distributions of AB model parameters are shown in Figure 5-3. The distributions of ε^0 and ε^1 exhibit some difference across the three types: they resemble exponential distributions in the PC-PC case, whereas they are uniformly or normally distributed in the HV-PC and PC-HV cases. Statistical tests suggest that ε^0 and ε^1 (within a given trajectory pair) is significant for the PC-HV case but insignificant for the other two cases. A larger sample is needed to further confirm the distribution difference.

(a)

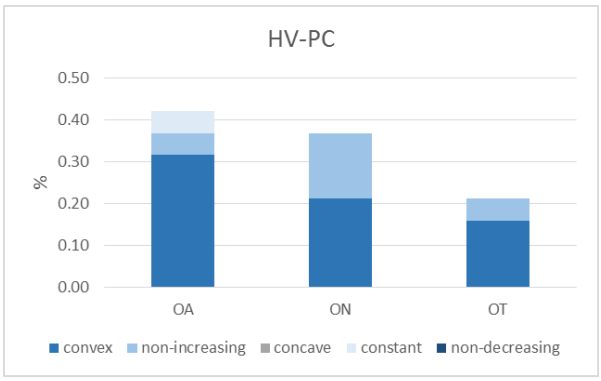

(b)

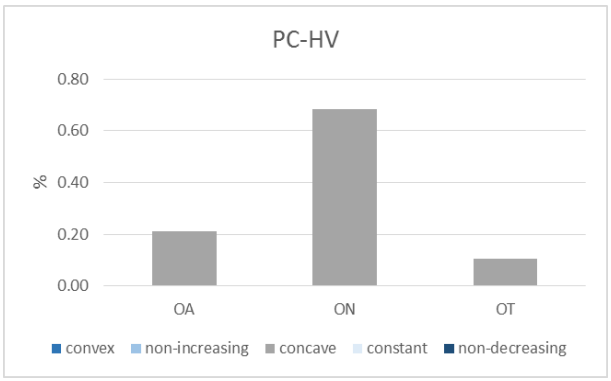

(c)

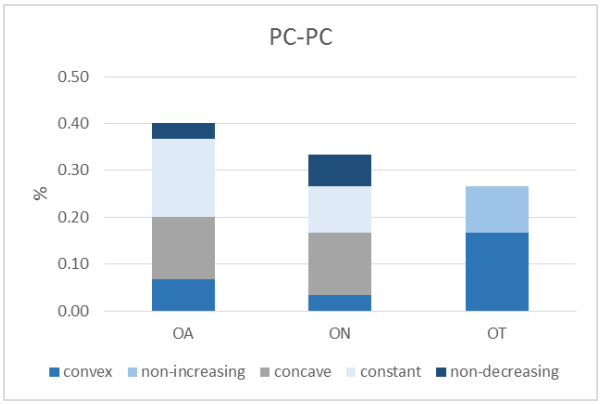

Figure 5-2: Driver category and reaction patterns for different CF types;

(a) HV-PC; (b) PC-HV; (c) PC-PC

(a)

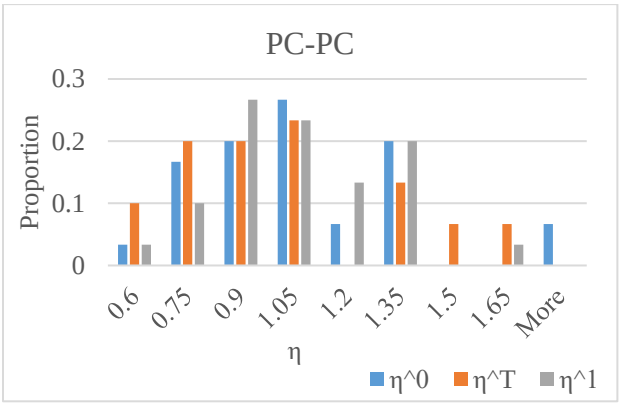

(b)

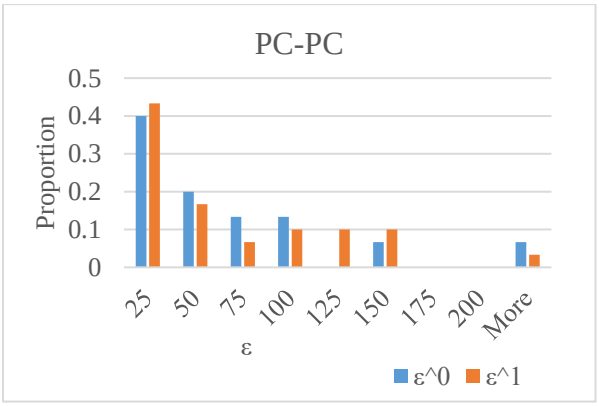

(c)

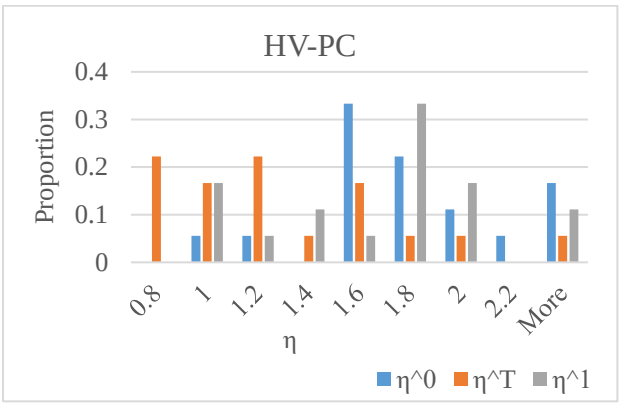

(d)

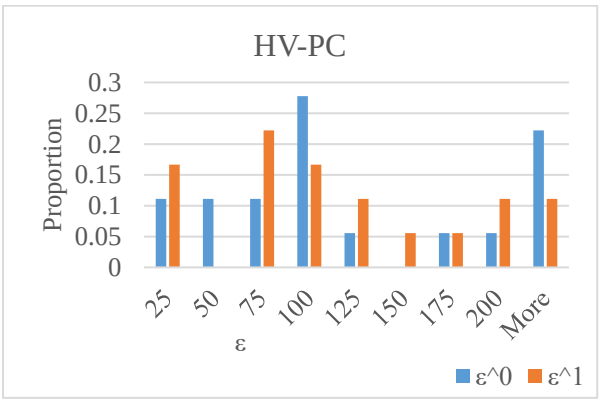

(e)

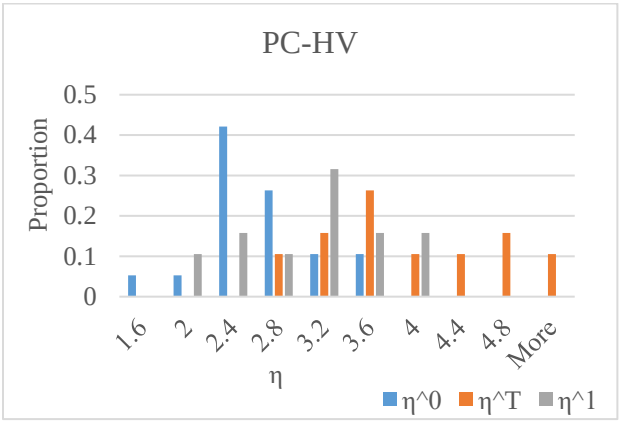

(f)

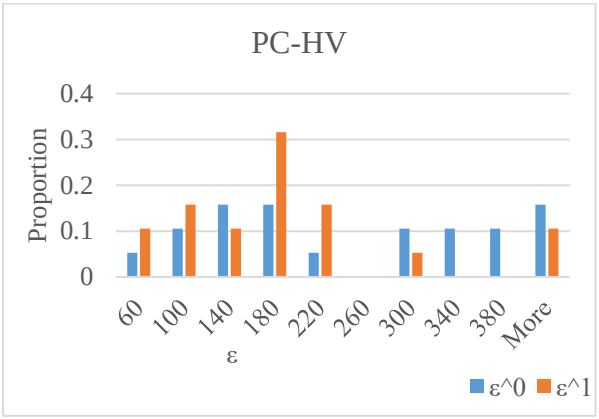

Figure 5-3: Distributions of AB model parameters (left column for η^0, η^T, and η^1, right column for ε^0 and ε^1): (a-b) PC-PC; (c-d) HV-PC; (e-f) PC-HV.

The above findings have an important implication for the development of oscillations. Notably, the dominant convex or non-increasing reaction patterns by the HV-PC pairs imply dampening of oscillations; i.e., a reduction of speed variation between the maximum and minimum speeds within a stop-and-go cycle. In contrast, the dominant concave reaction pattern by the PC-HV pairs implies the opposite effect, growth of oscillations, as verified in Chen et al. (2012a). The net effect will depend on the respective probabilities and magnitudes of these opposing effects since the composition of the two CF types would be basically even (one HV will be associated with one PC-HV and one HV-PC pair).

We performed a further empirical analysis to confirm this conjecture. An example of a dampening effect is presented in Figure 5-4. One can see in Figure 5-4 (a) that the HV, the follower, did not respond to the leader (a PC) to slow down, which resulted in a decreasing trend of τ (see Figure 5-4 (b)). The HV later responded to the acceleration, leading to a convex reaction pattern. For the example, the speed variation decreased from 20 ft/s for the leader to 10 ft/s for the follower. Overall, we found that a much larger proportion of the HV-PC pairs (42%) exhibited the dampening effect, compared to the PC-PC pairs and PC-HV pairs (10% and 16%); see Table 5-2. Moreover, the dampening effect was the greatest for the HV-PC pairs with the average reduction in speed variation of 9.4 ft/s, compared to 4.3 ft/s for the PC-PC pairs and 3ft/s in PC-HV pairs. In contrast, the PC-HV pairs had the highest probability to amplify oscillations (21%) as we conjectured, although the magnitude was not significantly different from other cases. We suspect that this is attributable to the heavy congestion, in which many vehicles already came to complete stop.

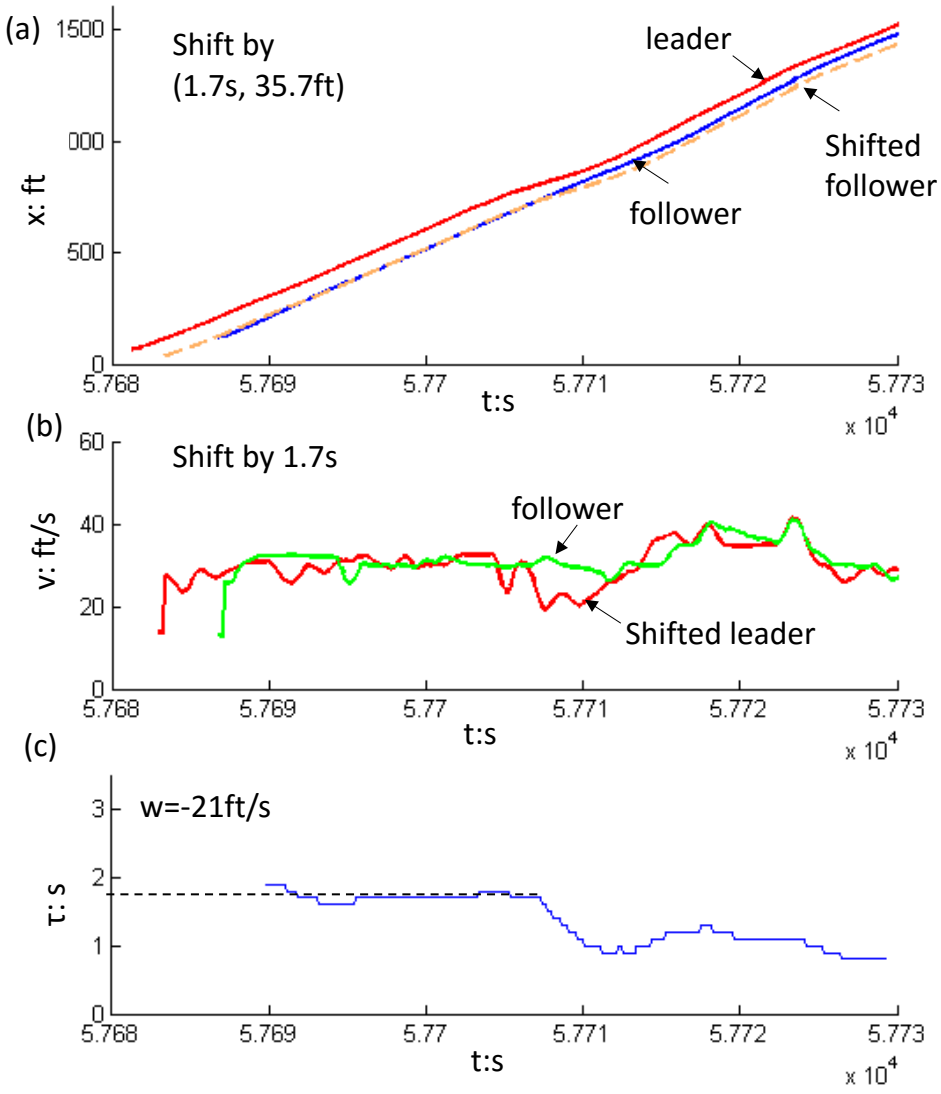

Figure 5-4: Dampening effect of TC pair (leader ID=416, follower ID=424 on lane 3 on I 80).

Table 5-2: Dampening and growth effect of CF pairs

	HV-PC (sample size: 19)		PC-HV (sample size: 19)		PC-PC (sample size: 30)	
	Magnitude: ft/s	Percentage	Magnitude: ft/s	Percentage	Magnitude: ft/s	Percentage
Dampen	9.38	42%	3.00	16%	4.33	10%
Grow	-5.00	5%	-3.50	21%	-4.40	17%
No change	0	53%	0	63%	0.00	73%

6 Heavy Vehicle Lane-Changing Characteristics

This chapter presents the analysis on the LC behavior around HVs. Specifically, we characterized LC rates around HVs (ahead and behind, and in and out) compared to PCs with the hypothesis that HVs induce different types and frequencies of LC around them.

6.1 Methodology

From the I 80 NGSIM dataset, we identified 82 HVs from lane 3 to lane 5. Lanes 1 and 2 were excluded since the sample size was too small while lane 6 involved very frequent LC maneuvers from the on-ramp and to the off-ramp. We also sampled PCs to establish the baseline. Particularly, systematic leftward LC maneuvers were observed for PCs in the dataset, and this will be taken into consideration for interpreting LC rates around HVs. The number of vehicles sampled is summarized in Table 6-1.

Table 6-1: Number of Vehicles Sampled

	I 80	
Lane	HV	PC
1	Not studied	
2	Not studied	
3	58	114
4	14	117
5	10	116
6	Not studied	
Total	82	347

In this project, we studied LC rates around subject vehicles, either HV or PC. (Note that the subject vehicles are not involved in the LC). We first identified three LC types that occurred ahead of a subject vehicle, as illustrated in Figure 6-1, where symbols denote the origins (open square and triangle) and the destinations (open circle) of LC maneuvers, and the arrows denote the LC direction. Particularly, C-ahead-out and C-ahead-in refer to the LC maneuvers that move out from the current lane (where the subject vehicle is traveling) and move into the current lane, respectively. A-ahead-out refers to the LC maneuvers that move outward (either to the right or left) from the adjacent lanes. Similarly, three LC types behind a subject vehicle were defined accordingly: C-behind-out (filled square), C-behind-in (filled circle), and A-behind-out (filled triangle). Furthermore, we considered the LC maneuvers that meet two criteria to assure that they could be influenced by the subject vehicle, which are illustrated in Figure 6-2: (1) the LC maneuvers occurred in the subject vehicle's influence zone, defined as the time-space domain within 10 seconds of the subject vehicle's trajectory; (2) there are at most two vehicles between the LC vehicle and the subject vehicle. When considering LC in the adjacent lanes (i.e., A-ahead-out and A-behind-out), the influence zone is obtained by projecting the subject vehicle's trajectory on the adjacent lanes. To quantify the LC effect around a subject vehicle, we define the LC rate as the number of eligible LC maneuvers per time and distance. The definition will enable comparison between trajectories in different length, time duration, and (or) traffic condition.

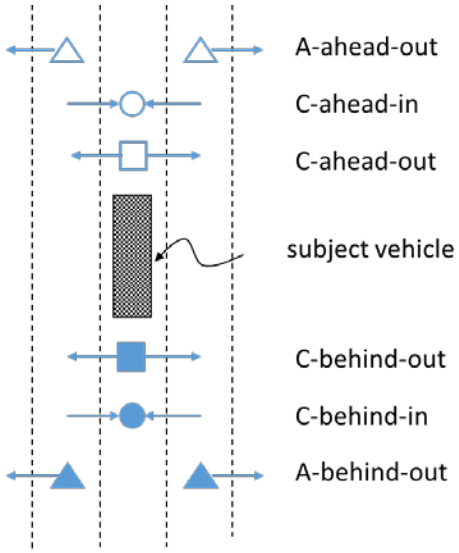

Figure 6-1: LC types

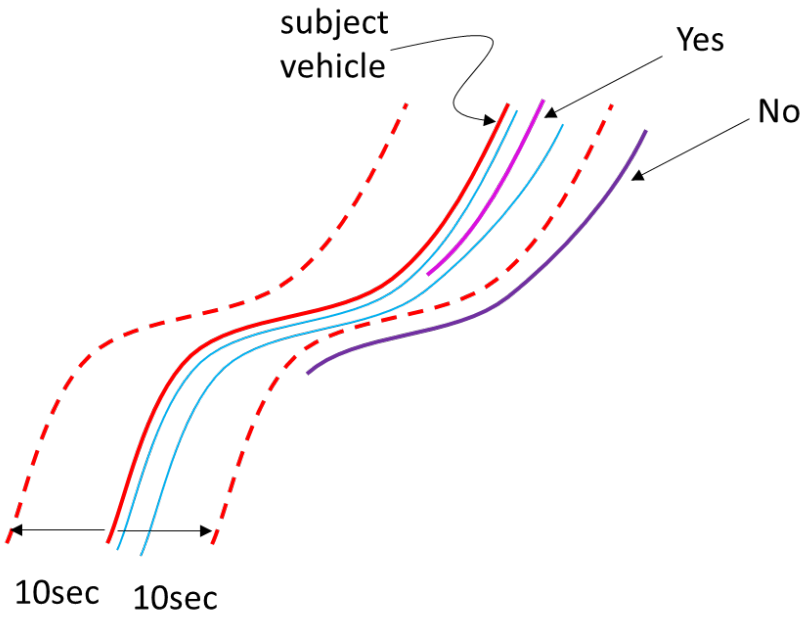

Figure 6-2: Criteria of effective LC

6.2 Results

Figure 6-3 presents the average LC rates for the six different LC types for HVs and PCs; see Table 6-2 for the more detailed lane-wise result. The main points are that (i) in general the LC rate of moving out is higher than moving in for PCs (e.g., LC rate out of the current lane (C-behind-out) is larger than the LC rate into the current lane (C-behind-in)); (ii) the difference between the LC rate in and out is much more significant for HVs compared to PCs, particularly when behind subject vehicles; and that (iii) the LC rates are generally lower involving HVs. The first finding suggests that there is systematic leftward lane-changing, which is attributed to the busy on-ramp on the right. The 2nd finding suggests that drivers are more likely to move out of the lane when they are behind HVs, which is consistent with the typical driving preference to avoid driving behind HVs. The third finding, however, has rather convoluted implications. On the one hand, a lower LC rate due to HVs implies better traffic stability since previous studies (Ahn & Cassidy, 2007; Mauch & Cassidy, 2002) have shown that LC maneuvers trigger traffic oscillations to form and grow. On the other hand, the presence of HVs can lead to underutilization of road capacity (capacity drop in near saturated conditions) since drivers are less likely to drive behind the HVs, leaving large gaps behind them (see the trajectories circled in Figure 6-4). These findings, together with the findings related to CF, suggest that HVs can help improve traffic stability directly (via dampening effect in CF) and indirectly (via reduced LC), though at the expense of possible capacity underutilization.

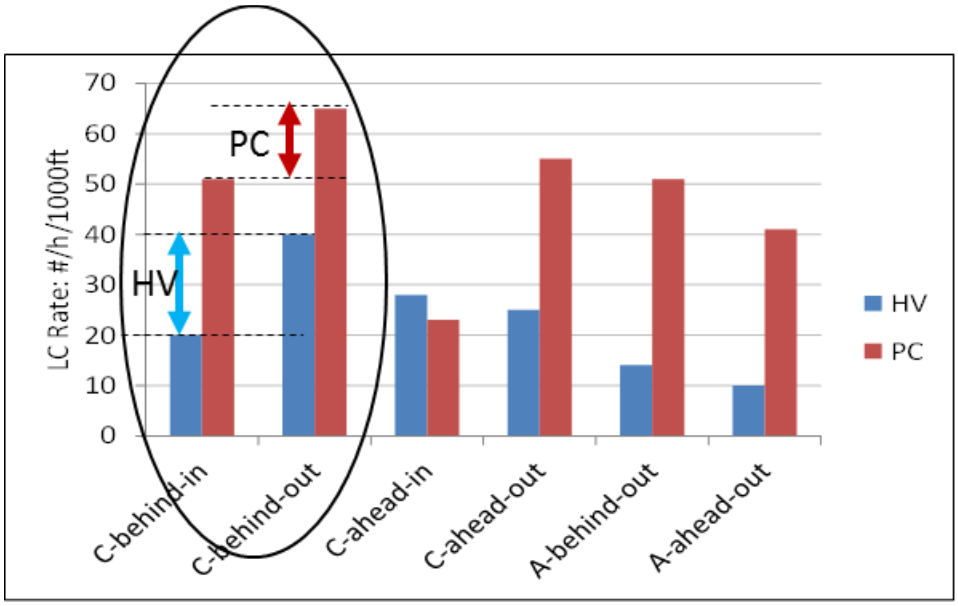

Figure 6-3: Average LC rates by LC type.

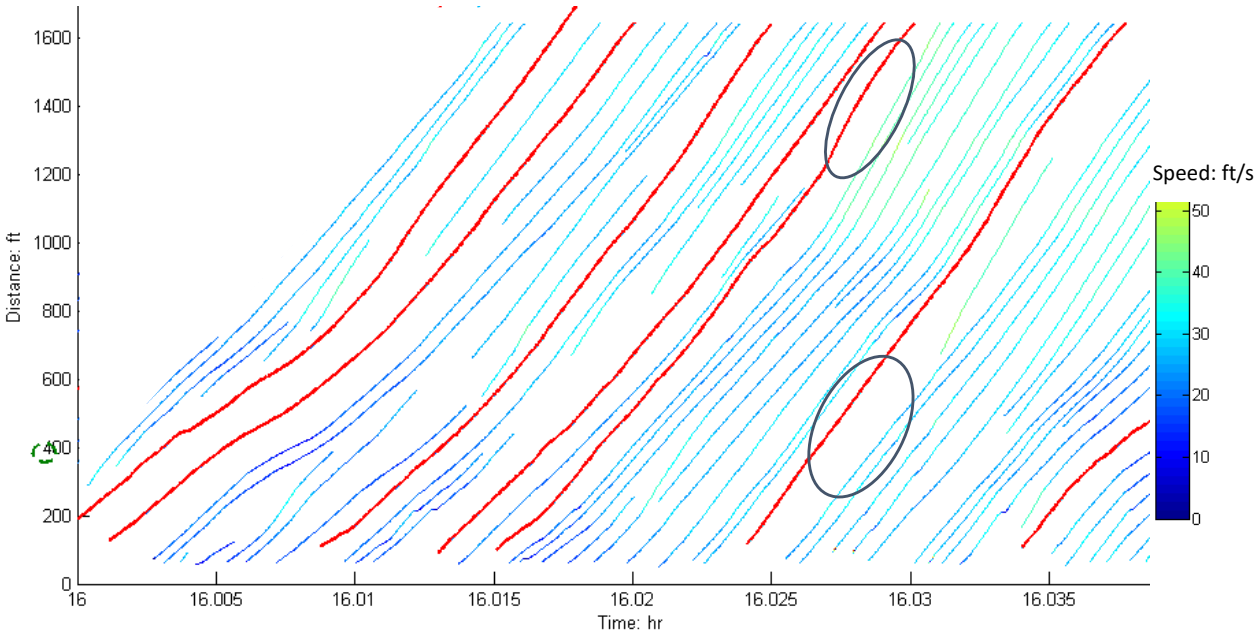

Figure 6-4: Example of large gap behind HV (I 80 lane 3. Red trajectories are HVs).

Table 6-2: LC rate (number/h/1000ft) for HV and PC

	C-behind-in	C-behind-out	C-ahead-in	C-ahead-out	A-behind-out	A-ahead-out
HV						
Lane3	9	32	23	29	7	5
Lane 4	43	59	50	17	25	27
Lane 5	48	61	26	15	39	14
Average	20	40	28	25	14	10
PC						
Lane3	50	47	16	32	26	24
Lane 4	31	47	27	58	45	53
Lane 5	74	99	26	76	82	46
Average	51	65	23	55	51	41

6.3 Summary of CF and LC Analysis

Chapter 5 and 6 conducted an empirical study of the CF behavior and LC effect of HVs. For the CF behavior, we found that different vehicle combination of CF pairs had very different features when experiencing stop-and-go traffic. PC-HV case showed the largest time gap (τ) and PC-PC the smallest. More importantly, HV-PC case showed significant dampening effect; i.e., they decreased the speed variation of the stop-and-go cycle. This effect was associated with the convex or non-increasing reaction pattern when the following HV responded to stop-and-go waves, in which HVs either responded late or decelerate in a milder way. For the LC effect, we found that HVs had the discouraging effect; i.e., they discouraged other vehicles to move in behind the HVs, which could be because of the high pressure when driving behind the HVs. This effect favors traffic stability by reducing potential disturbance imposed by LCs, but could undermine roadway utilization by creating large gap behind the HVs. It was also found that drivers were less likely to change lane when they were driving ahead of HVs, which could be because the traffic around HVs was relatively stable. Table 6-3 and Table 6-4 provide summaries for the key effects of the CF and LC behavior of HV, respectively. These results suggest that the effects of HVs on

the traffic flow are complex and a comprehensive evaluation, incorporating both CF and LC behavior, is needed.

Table 6-3: Summary on the effects of CF behavior of HV

CF behavior	**Capacity-drop**	**Source**	**Mechanism**
Dampening effect	-	HV-PC	HVs (convex, non-increasing reaction pattern) dissipate oscillations or prevent oscillations to form.
Growth effect	+	PC-HV	PCs (concave reaction pattern) cause oscillations to grow.

Table 6-4: Summary on the effects of LC behavior of HV

LC behavior	**Capacity-drop**	**Source**	**Mechanism**
LC Out > LC In	+	Large gap behind HVs	It is presumably less desirable to drive behind HVs.
Suppressed LC	-	Traffic around HVs	In general HVs discourage LCs around them.

7 Traffic Simulations

As an initial effort to evaluate the impact of HVs in traffic flow, simulations were conducted to examine the effects of HVs' CF behavior. Particularly, we focused on two typical types of bottleneck: rubbernecking and uphill segment. The former is a good representation of oscillatory traffic because a wide variety of sources of disturbances cause drivers to rubberneck and instigate stop-and-go oscillations. The latter uniquely affects HVs due to the sensitivity of HVs' performance to the grade.

7.1 Rubbernecking Bottleneck

The rubbernecking experiment used a similar setting to Chen et al. (2012a), in which traffic was simulated over a simple one-lane flat freeway segment with the length of 4.6 km; see Figure 7-1. Notice that a rubbernecking zone is located at [2.5km, 2.6km] from the most upstream point, where vehicles have a certain probability to slow down (i.e., rubberneck). Vehicles start to accelerate to free-flow speed after they leave the zone. To simplify the scenario and focus on the impact of HVs, we varied the HV proportion but fixed other simulation parameters. Namely, we assumed that vehicles have a probability of 6% to slow down, and the speed decreases by 40% after rubbernecking. To simplify the simulation, we also assumed that vehicles (both PCs and HVs) followed the same wave speed and they had a consistent maximum acceleration rate of 3 m/s^2. The HV proportion was varied from 0-25%. Measured parameters from the AB model (including driver category, reaction pattern, etc.) were used to reproduce CF behavior of PCs and HVs. The simulations produced trajectories of each individual vehicle. Each parameter setting had 20 runs with random seeds.

Based on simulation results, we measured the discharge flow 2km downstream of the rubbernecking zone. Figure 7-2 shows the measured flow. Notice that the figure shows a decreasing trend as the HV proportion increases. This is not surprising since the CF spacing required by HV-PC and PC-HV is much larger than PC-PC. Therefore, an equivalent factor was used to normalize different spacing level to the

standard PC unit. Namely, the equivalent factor, denoted by ET_{HV-PC}, was obtained by calculating the ratio of time headway in saturation condition for HV-PC and PC-PC, which was reduced to the ratio of τ_0 for HV-PC and τ_0 in PC-PC since the same wave speed was used. The equivalent factor for PC-HV, $\mathrm{ET}_{\mathrm{PC-HV}}$ was obtained in a similar way. The equivalent factors were estimated as: $\mathrm{ET}_{\mathrm{HV-PC}} = 1.8$ and $\mathrm{ET}_{\mathrm{PC-HV}} = 2.4$. Figure 7-3 shows the normalized discharge flow, which displays an increasing trend. Note that in steady traffic conditions (i.e., no oscillations), the normalized discharge flow is expected to remain constant with respect to the HV proportion. Thus, this increase in discharge flow is attributed to the unique impact of HVs in oscillatory traffic. In particular, we conjecture that it is because HV traffic decreases the probability of oscillation formation and growth and consequently reduces the overall capacity-drop. This is supported by the following evidence. We found that the period of oscillations increased with HV proportion; see Figure 7-4 for average period plot and Figure 7-5 and Figure 7-6 for trajectory snapshot for HV=0 and HV=25%. On close examination, it was found that some oscillation precursors (triggered by either PC or HV rubberneckers) were dissipated by HVs or their immediate followers; see case 1 labeled in Figure 7-7 for an example. Even partially-formed oscillations were dissipated; see case 2. Such dissipation is consistent with the dampening effect observed in the empirical data revealed in Chapter 5, which was attributed to the large spacing maintained by HV-PC pairs and their reaction patterns (mostly convex or non-increasing). With less frequent oscillations, the effect of capacity-drop associated with oscillations is smaller; i.e., the normalized discharge flow is larger.

In summary, our simulations show the impact of HV's CF behavior in oscillatory traffic. HVs in congested traffic streams lead to (1) more stable traffic (i.e., less frequent oscillations) and (2) smaller capacity-drop. In terms of roadway utilization, despite (2), the measured discharge flow (in vehicle/hour) decreases with HV proportion due to large spacing maintained by HVs and their immediate followers.

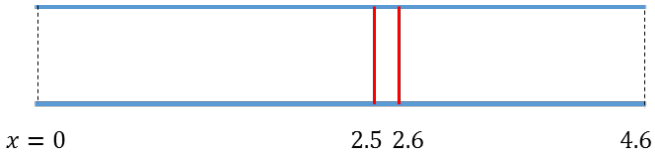

Figure 7-1: Simulation sketch

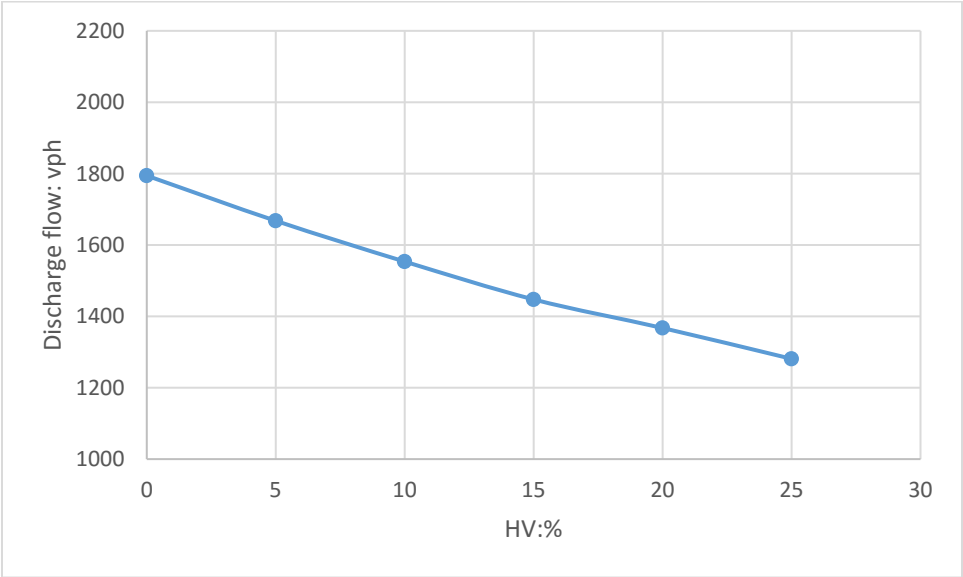

Figure 7-2: Measured discharge flow vs. HV proportion

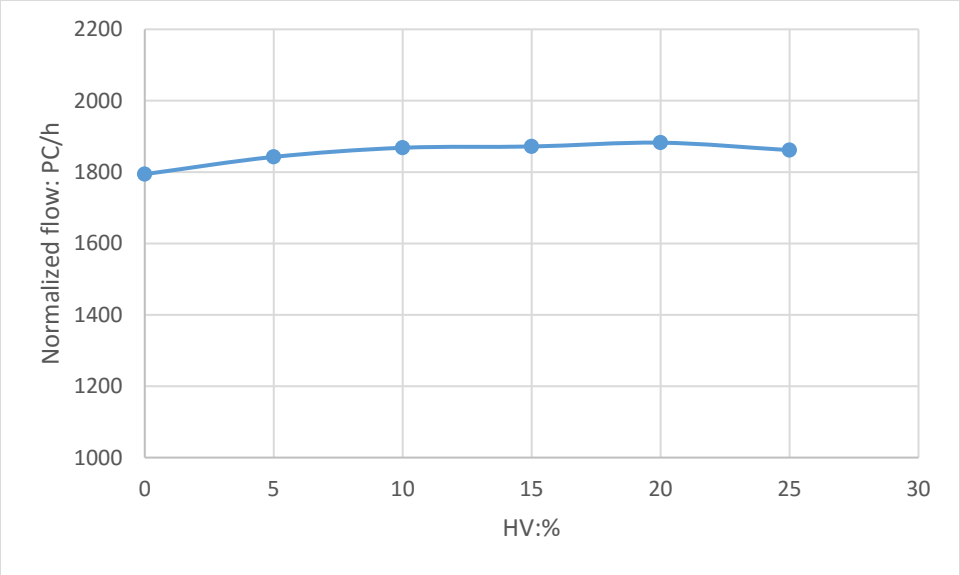

Figure 7-3: Normalized discharge flow vs. HV proportion

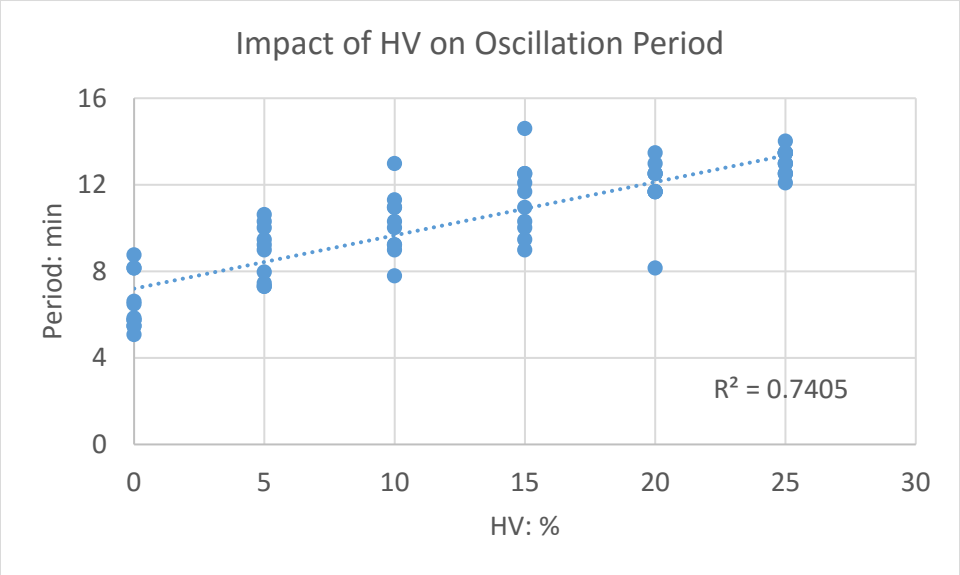

Figure 7-4: Traffic oscillation period vs. HV proportion

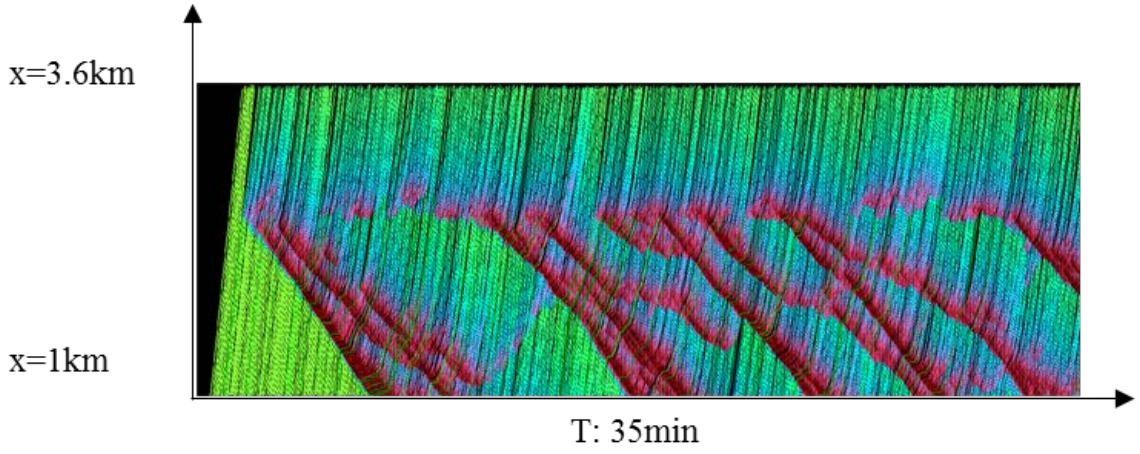

Figure 7-5: Traffic condition with HV proportion=0

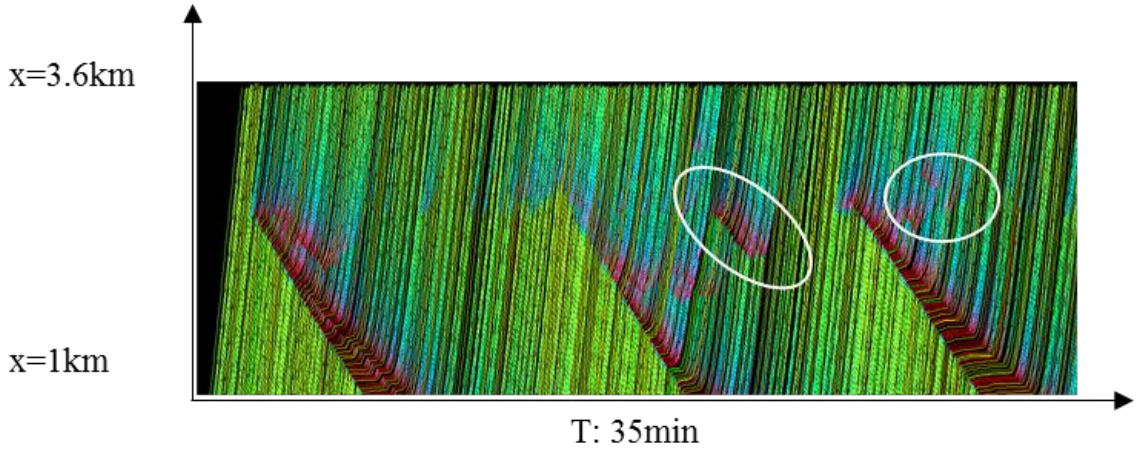

Figure 7-6: Traffic condition with HV proportion=20%

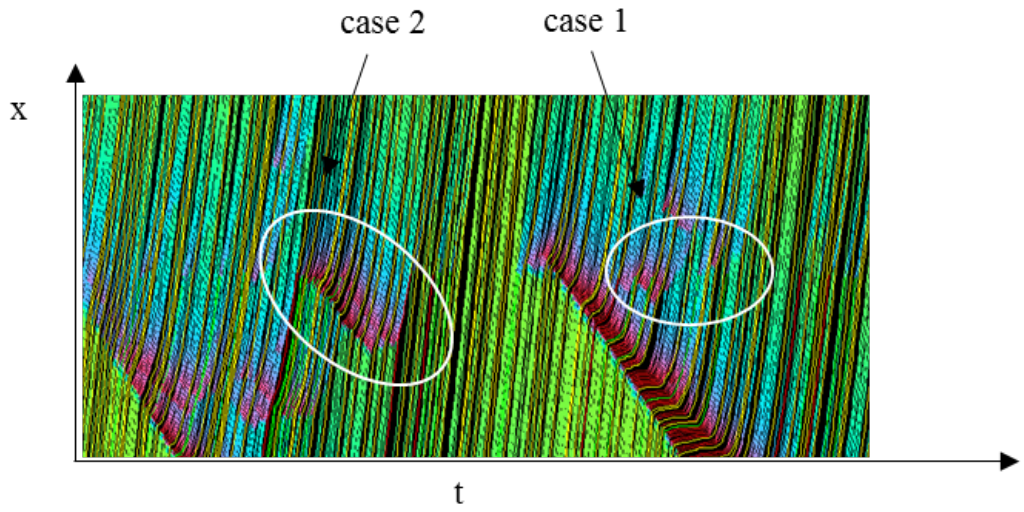

Figure 7-7: Traffic dynamics zoomed in from Figure 7-6

7.2 Uphill Bottleneck

In this simulation, we studied a highway bottleneck caused by an uphill segment. Particularly, we aimed to study two cases: (1) the pure effect of grade and (2) the compound effects when the grade is coupled with variable driver characteristics. For this purpose, we simulated a one-lane highway segment with the length of 6km; see Figure 7-8. Notice that there is an extended uphill segment located at [2km, 4km] with grade G in percentage, and other segments are flat. Next, we introduce the model to capture vehicles' mechanics on grade and then the simulations for the two cases.

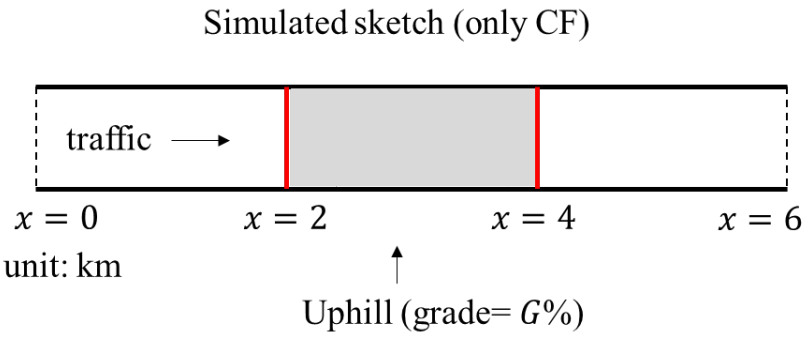

Figure 7-8: Roadway Sketch for Uphill simulations

7.2.1 Vehicle mechanics on grade

To capture vehicles' mechanics on hills, we adopted FHWA's kinematic vehicle model (FHWA, 2000), which describes a vehicle's acceleration in the following way:

$$a(v) = a_m \left[1 - \frac{v}{u}\right] - \frac{gG}{100}, \tag{10}$$

where $a(v)$ is the acceleration at speed v, a_m is the maximum acceleration rate of a vehicle, u is the free-flow speed, g (=9.8 m/s^2) is the gravity constant, and G is the grade in percentage. Clearly, the 1st term

in the equation ($a_m\left[1-\frac{v}{u}\right]$) denotes a vehicle's acceleration capability constrained by the vehicle's mechanic feature, while the 2nd term denotes the deceleration imposed by the gravity. Particularly, the maximum acceleration rate (a_m) is an important mechanic feature of the vehicle, which is determined by the horsepower. In addition to a_m, a vehicle's acceleration varies with the real-time speed, which reaches the maximum at complete stop ($v = 0$) and becomes zero at free-flow speed. By contrast, the deceleration imposed by gravity only depends on the grade. The balance of these two terms determines the actual acceleration of a vehicle. Specifically, a vehicle entering the uphill segment at free-flow speed u will be forced by the gravity to slow down until the gravity is compensated by its acceleration capability and the vehicle reaches the cruise speed (i.e., $a(v) = 0$), which is given as follows:

$$v_{cruise} = u\left(1-\frac{gG}{100a_m}\right). \tag{11}$$

After passing the uphill segment, a vehicle will start to accelerate to recover to free-flow speed.

Notably, HVs usually have smaller maximum acceleration rate (a_m) due to the weight and size of the vehicles, compared to PCs. Thus, the grade has a much more profound on HVs. For example, the cruise speed is much smaller with a smaller a_m. To capture this effect, we assumed that PCs have $a_m = 3m/s^2$ and HVs only have 1/3 of the acceleration capability with $a_m = 1m/s^2$.

7.2.2 Pure Effect of Grade

In this simulation setting, we aimed to focus only on the effect of grade. For this purpose, it is assumed that vehicles desire to follow Newell's model (Newell, 2003) but are still constrained by the impacts of grade. For the model's parameters, since we had a small sample from empirical measurement, we used the method of sample enumeration (Ben-Akiva and Lerman, 1985). Particularly, for each CF type, we

constructed a sample matric for η^0 using the empirical measurement result in Chapter 5. When a vehicle was generated in the simulation, depending on the CF type, it was assigned with a value for η^0 that was randomly drawn from the corresponding sample matric of the CF type. Thereafter, the vehicle would attempt to maintain the same η^0 level regardless of the traffic condition; i.e., it aimed to follow Newell's CF model.

In the simulations, we varied the grade from 0 to 7% and the HV proportion from 0 to 25%. Each parameter combination was repeated over 20 runs with random seeds. Figure 7-9 and Figure 7-10 show the absolute discharge flow in vehicle per hour and the normalized flow in PC/h. Figure 7-11 replotted the relationship between normalized discharge flow and grade. From the results, we obtained the following remarks:

> R-1: When the grade was positive (i.e., $G > 0$), the normalized discharge flow decreased with HV proportion, but quickly converged mostly after $HV > 5\%$; see the plot in Figure 7-10.
>
> R-2: The overall normalized discharge flow level decreased with the grade (see the curves corresponding to different grade levels in Figure 7-10).
>
> R-3: The impact of grade was much more profound for HVs than PCs. Particularly, for PCs the normalized discharge flow didn't decrease until the grade reaches 3%, and the overall reduction was 20% at the grade of 7%. By contrast, for HVs, the grade's effect was significant even at 1% and the normalized discharge flow reduced by 44.5% at grade 7% even when there were only 5% of HVs; see Figure 7-11.

Regarding R-1, the former part of the result was expected because HVs slow down on the uphill segment and create voids due to the limited acceleration capability. Since the acceleration capability was much smaller for HVs, the voids were much larger for HVs than PCs; i.e., the discharge flow was much smaller when HVs are present. This is also illustrated in the trajectory plot of Figure 7-12. The quick

convergence, however, is puzzling. We suspect that it is due to complex interactions between grade, vehicle mechanic, and variable driver characteristics, and further studies are needed to gain better insight.

R-2 was expected as when the grade was larger, it induced larger voids in the HVs. For example, the cruise speed would be smaller; as shown in Eqn. (11). Similarly, the result of R-3 was straightforward as implied by Eqn. (10-11). In general, the grade effect would be much more significant in vehicles with smaller a_m.

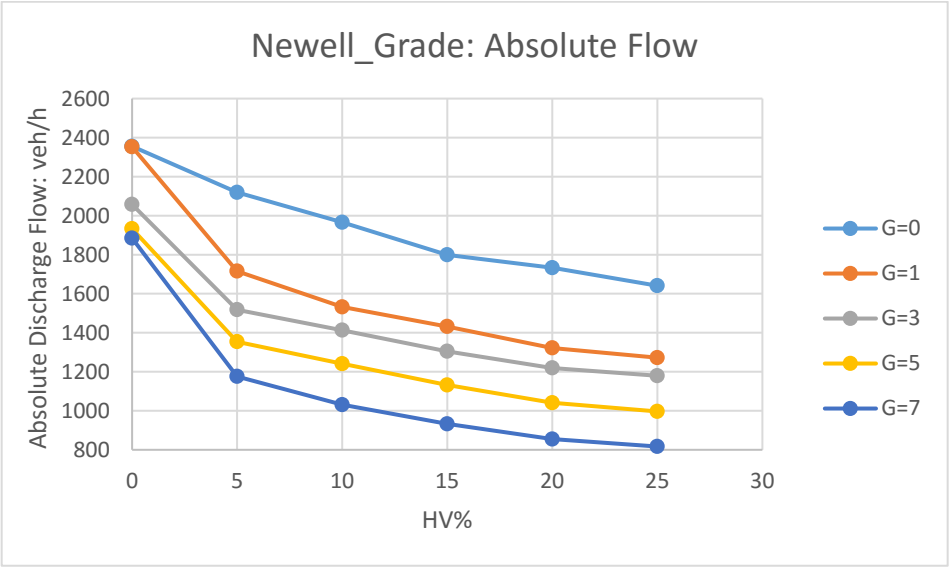

Figure 7-9: Absolute discharge flow in Newell's CF model (legend denotes the G value)

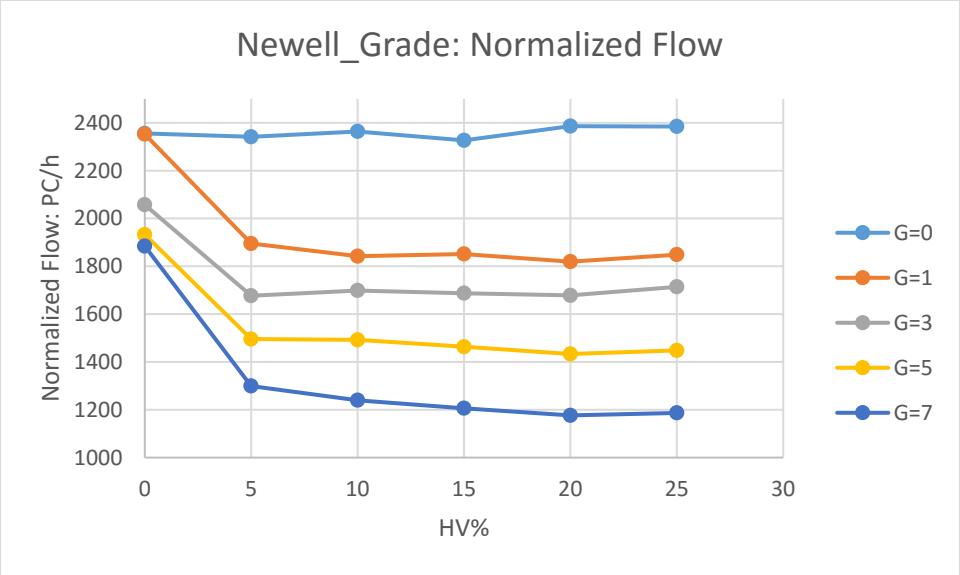

Figure 7-10: Normalized discharge flow in Newell's CF model (legend denotes the G value)

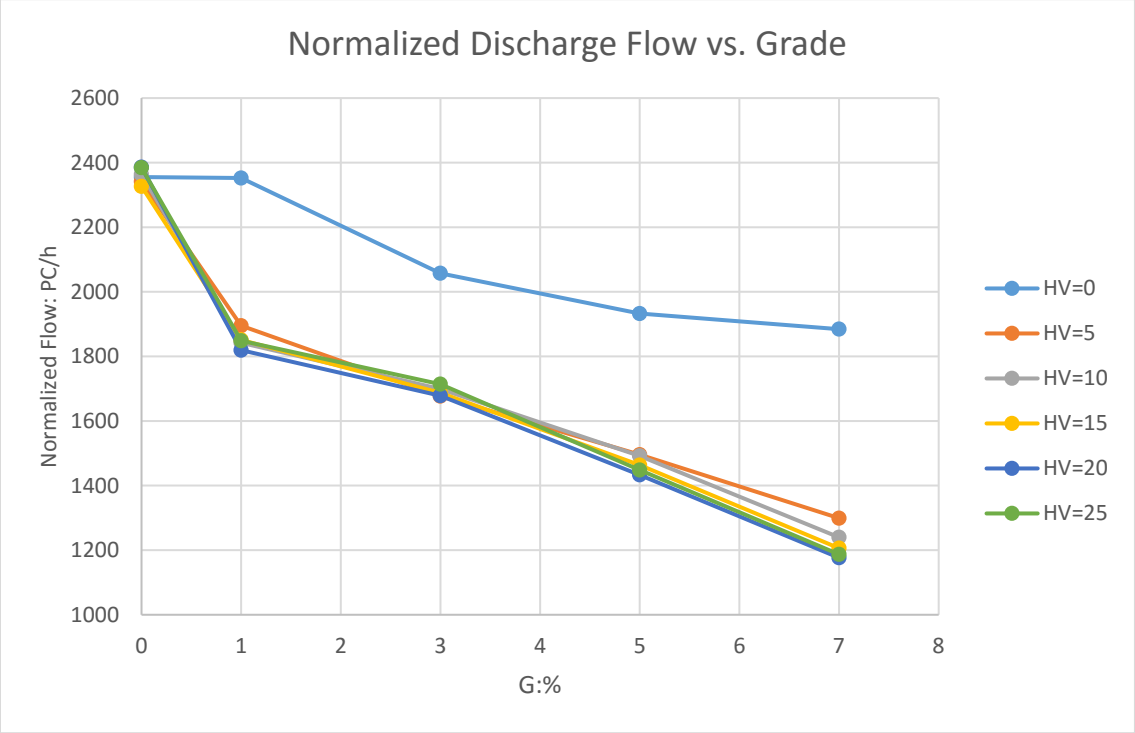

Figure 7-11: Normalized discharge flow vs. grade -Newell's CF model (legend denotes the HV proportion)

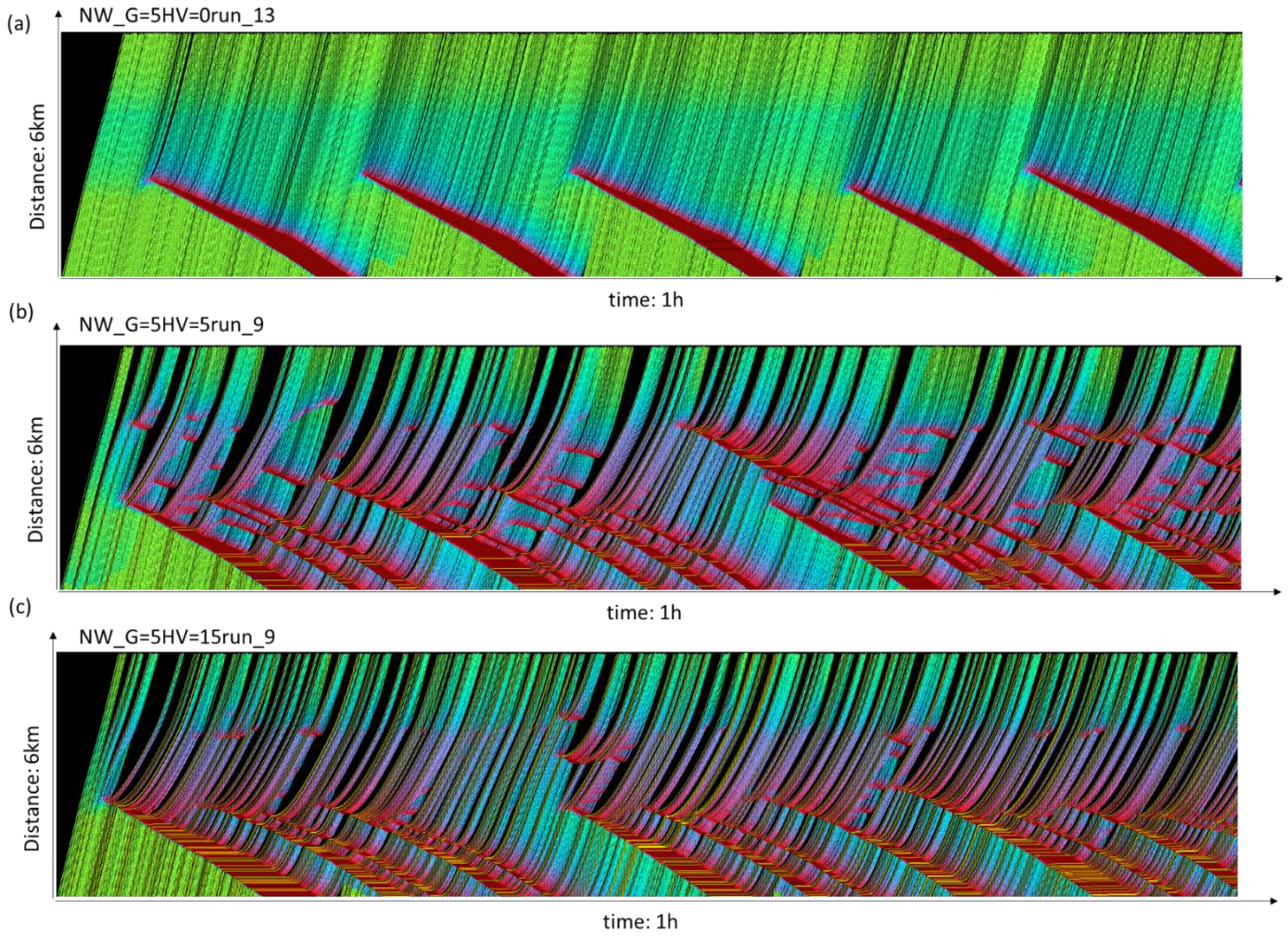

Figure 7-12: Trajectory plots: Newell's CF model in uphill segment

7.2.3 Compound Effects of Grade and Variable Vehicle Characteristics

In this simulation experiment, we studied the compound effects of grade and variable driver characteristics. For this purpose, we assumed that vehicles follow the AB model. Particularly, in the generation of model parameters, we applied the same sample enumeration method, but the parameters

include all five parameters of the AB model (η_{i+1}^0, η_{i+1}^T, η_{i+1}^1, ε_{i+1}^0, ε_{i+1}^1) (note that ε_{i+1}^0 and ε_{i+1}^1 were assumed to be the same since statistic test showed that the difference was not significant).

Similar to the experiment of grade-only, we varied the grade from 0 to 7% and the HV proportion from 0 to 25%. Each parameter combination was repeated over 20 runs with random seeds. Figure 7-13 and Figure 7-14 showed the absolute discharge flow in vehicle per hour and the normalized flow in PC/h. Notice that the results are similar to the previous case when Newell's model was used and remarks (R-1 to R-3) held for this case too. This is not surprising given the prevalent effect of grade and HVs. A comparison of the normalized discharge flow in the two cases was shown in Figure 7-15. Notably, when the HV proportion was positive, the flow difference (normalized discharge flow from Newell's model subtracted by the discharge flow from AB model) decreased with the grade. This could be because when the grade was significant, the grade effect was dominant and the variable driver characteristics played a marginal role, which led to similar results from the two models. The figure also suggested that with given grade level, the flow difference decreased with the HV proportion. This was because when the HV proportion was significant, the traffic became too congested (due to the high proportion of HV) and traveled at the cruising speed of HVs, such that the variable driver characteristics only played a marginal role. In fact, this could been seen by comparing the trajectories in the two cases as shown in Figure 7-12 and Figure 7-16 respectively. Notice that for the same grade (5%), when HV proportion was 0, there were more disturbances in the traffic produced from AB model because disturbances were more likely to grow and get amplified in the AB model. However, when the HV proportion was 15%, the bottleneck (i.e., uphill segment) was mostly at the cruising state of HVs, and the difference between the two models was very small.

The simulation result suggests that the traffic dynamics on the uphill result from the compound effects of grade, vehicle's mechanic features, and driver's variable characteristics. The interactions were very complex. The mechanisms and quantitative formulations are left for future studies.

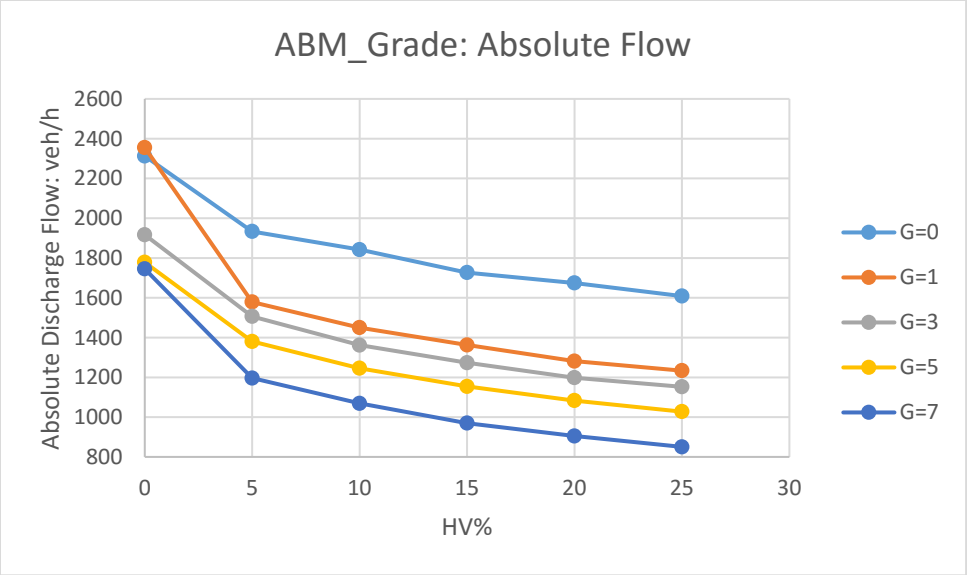

Figure 7-13: Normalized discharge flow in AB model (legend denotes the G value)

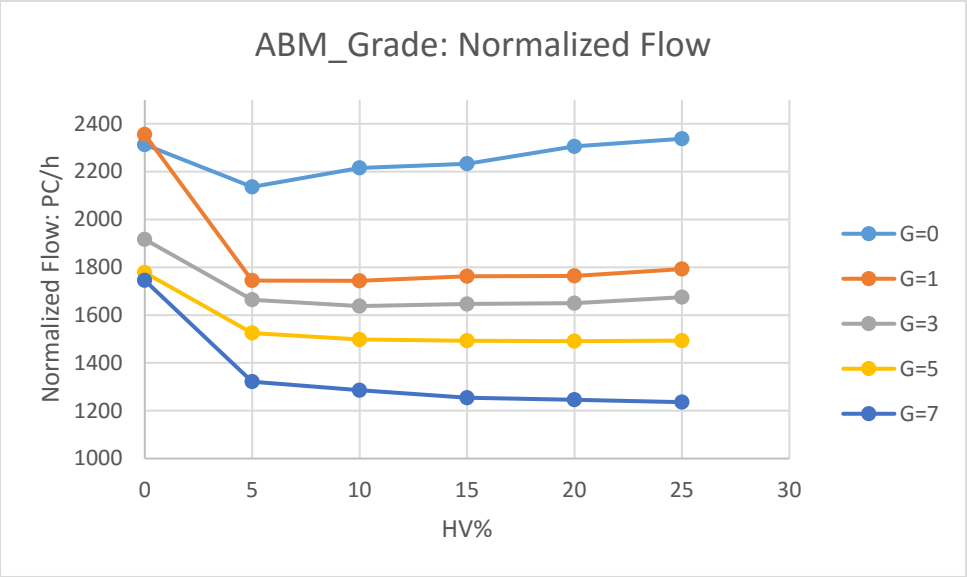

Figure 7-14: Absolute discharge flow in AB model (legend denotes the G value)

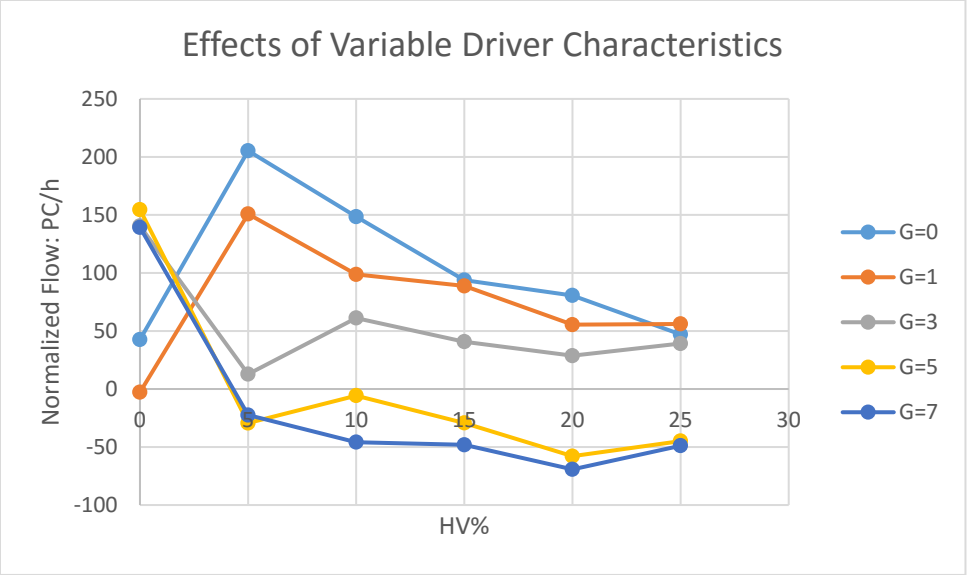

Figure 7-15 : Difference of normalized discharge flow in Newell's CF model and AB model (legend denotes the G value)

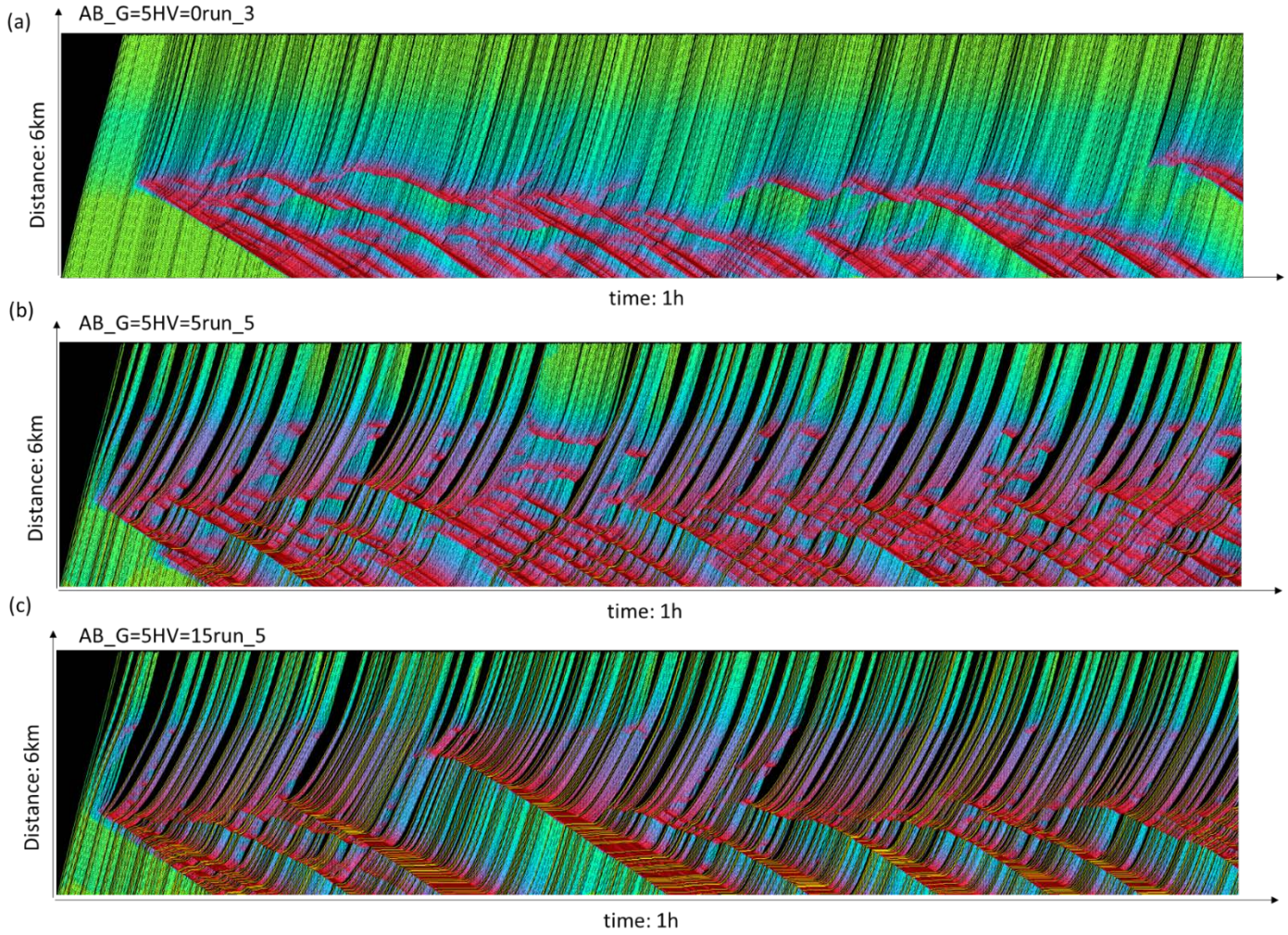

Figure 7-16: Trajectory plots: AB model in uphill segment

8 Conclusions and Discussions

In this project, three well-known CF models, Newell's model, Gipps' model, and IDM, were calibrated using real trajectory data for HVs. Calibration results suggest that the model performance, in terms of errors, varies with time resolution of data in calibration. The performance of IDM deteriorated with time resolution (i.e., the errors increased), but Newell's model improved as the time resolution increased. Gipps' model seems complex, with the errors showing a convex relationship with the time resolution. With the time resolution of 1s, a typical magnitude used in practice, IDM had smaller errors (5%) than Newell's model and Gipps' model (the latter two have similar errors, about 8-13%), but Newell's model eventually surpassed IDM as the time resolution continues to increase. Our analysis also suggests that model parameters show different sensitivity levels to the time resolution. Newell's model was insensitive to the time resolution, and the calibrated parameter values remained stable across different resolution levels, which is a desired property for CF models. However, a large proportion of parameters in IDM and Gipps' model varied significantly as the resolution changes, which presents a challenge for calibration. After a comprehensive evaluation of model's advantage and limitations, Newell's model turns out to be advantageous because (1) the model structure is extremely simple while it produces reasonable performance, (2) the calibrated parameters are not sensitive to the time resolution used in calibration, (3) the model parameters have clear physical meaning and can be measured directly from empirical data, and (4) extended models based on Newell's model (Laval and Leclercq, 2010; Chen et al., 2012a) had demonstrated the capability to capture the formation and development mechanisms of stop-and-go oscillations.

For the next phase of the project, the AB model (Chen et al., 2012a), an extended Newell's model, was modified to further examine the effects of HVs' CF behavior on two key traffic phenomena: capacity drop and stop-and-go oscillations. This extended Newell's model was selected over IDM because (1) it is much simpler, yet effective in describing the key traffic phenomena, (2) the model parameters have

clearer physical meaning that could be measured directly from the real data, and (3) most importantly, the model described driving behavior at the individual vehicle level, which was critical to unveiling mechanisms of evolution of oscillations and their impact on capacity-drop.

Based on the AB model, an empirical analysis was conducted to better understand the CF and LC behavior of HVs. For CF behavior, we measured the parameters of the AB model for three CF combinations, HV-PC, PC-HV, and PC-PC. It was found that the PC-HV pairs showed the largest average time gap (τ) and the PC-PC pairs showed the smallest. More importantly, the HV-PC case showed a significant dampening effect by decreasing speed variations during stop-and-go cycles. This effect was associated with the convex or non-increasing reaction pattern of HVs, as a result of responding late to a stop-and-go wave or decelerating in milder way. On the other hand, HVs maintained much larger spatial gap, resulting in lower flow (measured in veh/h). For the LC effect, it was found that HVs had a discouraging effect; i.e., vehicles were less likely to insert behind HVs presumably due to less desirable CF conditions (e.g., limited sight distance). This effect favors traffic stability by reducing potential disturbances instigated by LCs, but could undermine roadway utilization by creating a large gap behind the HVs. For both CF and LC behavior, there were behavioral aspects that could favor and undermine the traffic flow efficiency and the interaction was complex. A comprehensive evaluation of HVs integrating both CF and LC behavior is needed in future research.

Based on the results of empirical studies, this study conducted simulations to study the impacts of the CF behavior of HVs in two typical types of highway bottleneck: rubbernecking and uphill segment. In the rubbernecking experiment, it was found that HVs reduced the formation and growth of traffic oscillations. This resulted in reduced overall capacity-drop: the normalized bottleneck discharge flow in PC/h increased with HV proportion. In the uphill experiment, it was found that restrained acceleration due to roadway grade could cause a significant reduction in discharge flow and that the effect was much more profound for HVs than PCs. It was also found that the effect of variable driver characteristics diminished

with the grade and HV proportion. Lastly, with given positive grade, the effects of HV proportion quickly diminished and became marginal, which was a puzzling result. It is suspected that it is a result of complex interactions among grade, vehicle mechanics, and variable driver characteristics. Further studies are needed to elucidate these interactions.

In the simulations, considering both CF and LC behavior, it was found HVs led to more stable traffic and produced compound effects on flow efficiency: they required large CF gaps, which resulted in lower flow (in vehicle/hour); on the other hand, they mitigated traffic oscillations, thereby diminishing capacity drop and improved the normalized discharge flow (in PC/h). Such effects were particularly profound in oscillatory traffic, such as highway with rubbernecking bottlenecks. On highway uphill segments, HVs led to significant reduction in discharge flow (in PC/h) because they had limited acceleration capability. The effect of variable driving characteristics seemed to become marginal when the grade or (and) HV proportion was significant.

Due to the data limitation, this research was unable to build a meaningful LC model. Further research is needed to address this problem and then integrate both the CF and LC models to have a comprehensive evaluation of HV's impact. Also, the CF behavior of heavy vehicle-following-heavy vehicle was not studied due to the lack of reasonable sample size. A future study is needed to complete the analysis of the HV behavior. Last but not least, this study examined only one site and comparison across different sites is needed to further generalize the findings. We will investigate these problems in future research.

Acknowledgement

This research was sponsored by CFIRE: National Center for Freight & Infrastructure Research & Education.

References

1. Aghabayk, K., Sarvi, M., and Young, W. Understanding the Dynamics of Heavy Vehicle Interactions in Car-Following. Journal of Transportation Engineering, Vol. 138, No. 12, 2012, pp.1468-1475.

2. Ahmed, K. I. Modeling Drivers' Acceleration and Lane-Changing Behavior. Ph.D. thesis. Massachusetts Institute of Technology, Cambridge, 1999.

3. Ahn, S., Cassidy, M.J., Laval, J. Verification of Simplified Car-following Theory. Transportation Research Part B, Vol. 38, 2004, pp. 431-440.

4. Ahn, S., and Cassidy, M.J. Freeway Traffic Oscillations and Vehicle Lane-changing Maneuvers. The 17th International Symposium on Transportation and Traffic flow Theory, 2007, pp. 691–710.

5. Barceló, J., Casas, J.. Dynamic Network Simulation with AIMSUN Simulation Approaches. In: Kitamura, R., Kuwahara, M. (Ed.), Simulation Approaches in Transportation Analysis. Springer, 2005.

6. Ben-Akiva, M., Lerman, S.R., 1985. Discrete Choice Analysis: Theory And Application to Travel Demand. MIT Press.

7. Brockfeld, E., R. D. Kühne, and P. Wagner. Calibration and Validation of Microscopic Traffic Flow Models. In Transportation Research Record: Journal of the Transportation Research Board, No. 1876, 2004.

8. Cate, M. A., and Urbanik II, T. Another View of Truck Lane Restrictions. Transportation Research Record: Journal of the Transportation Research Board, No. 1867, 2004, pp. 19–24.

9. Chen, D., Laval, J., Zheng, Z., and Ahn, S. A Behavioral Car-following Model that Captures Traffic Oscillations. Transportation Research Part B, Vol.46, 2012a, pp. 744–761.

10. Chen, D., Laval, J.A., Ahn, S., and Zheng, Z. Microscopic Traffic Hysteresis in Traffic Oscillations: a Behavioral Perspective. Transportation Research Part B, Vol. 46, No. 10, 2012b, pp. 1440–1453.

11. Chen, D., Ahn, S., Laval, J., and Zheng, Z. On the Periodicity of Traffic Oscillations and Capacity Drop: The Role of Driver Characteristics, Transportation Research Part B, Vol. 59, 2014, pp. 117–136.

12. Chiabaut, N., Leclercq, L., and Buisson, C. From Heterogeneous Drivers to Macroscopic Patterns in Congestion. Transportation Research Part B, Vol. 44, 2010, pp. 299-308.

13. Duret, A., Ahn, S., and Buisson, C. Passing Rates to Measure Relaxation And Impact of Lane-Changing In Queue. Computeraided Engineering and Infrastructure Engineering 26 (4), 2011, pp. 285–297.

14. EI-Tantawy, D., M.J. Roorda, and B.Abdulhai. Safety Evaluation of Truck Lane Restriction Strategies using Microsimulation Modeling. Transportation Research Record: Journal of the Transportation Research Board, No. 2099, 2009, pp. 123-131.

15. FHWA. The Capability And Enhancement of VDANL And TWOPAS for Analyzing Vehicle Performance on Upgrades And Downgrades Within IHSDM, 2000.

16. Gan, A., and Jo, S. Operation Performance Models for Freeway Truck-lane Restrictions. Florida Department of Transportation, Project No. BD-015-01, 2003.

17. Gipps, P. G. A Behavioural Car-following Model for Computer Simulation. Transportation Research Part B, Vol. 15, No. 2, 1981, pp.105-111.

18. Goldberg, D. E. Genetic Algorithms in Search, Optimization and Machine Learning. Addison-Wesley, 1989.

19. Grenzeback, L., R., Reilly, W. R., Roberts, P. O., and Stowers, J. R. Urban Freeway Gridlock Study: Decreasing the Effects of Large Trucks on Peak-period Urban Freeway Congestion. Transportation Research Record: Journal of the Transportation Research Board, No. 1256, 1990, pp. 16-26.

20. Hoel, L. A., and J. L. Peek. A Simulation Analysis of Traffic Flow Elements for Restricted Truck Lanes on Interstate Highways in Virginia. Virginia Transportation Research Council, 1999.

21. Jasek, D., M. A. Shafer, D. L. Picha, and T. Urbanik II. Guidelines for Truck Lane Restrictions in Texas. Texas Transportation Institute, Research Report 1726-S, 1997.

22. Jo, S., Gan, Al., and Bonyani, G. Impacts of Truck-Lane Restrictions on Freeway Traffic Operations. The 82nd Annual Meeting of the Transportation Research Board, 2003.

23. Kesting, A., M. Treiber, M. Schönhof, and D. Helbing. Adaptive Cruise Control Design for Active Congestion Avoidance. Transportation Research Part C, Vol. 16, No. 6, Dec. 2008, pp. 668–683.

24. Kesting, A., M. Treiber, M. Schönhof, and D. Helbing. Extending Adap- tive Cruise Control to Adaptive Driving Strategies. Transportation Research Record: Journal of the Transportation Research Board, No. 2000, Transportation Research Board of the National Academies, Washington, D.C., 2007, pp. 16–24.

25. Kerner, B. S., and Rehborn, H. Experimental Properties of Complexity in Traffic Flow, Physical Review E, Vol. 53, No. 5, 1996, pp. R4275-4278.

26. Laval, J.A., and Leclercq, L. A Mechanism to Describe the Formation And Propagation of Stop-And-Go Waves in Congested Freeway Traffic. Philosophical Transactions of the Royal Society A, Vol. 368, Iss. 1928, 2010, pp. 4519–4541.

27. Lighthill, M.J., and Whitham, G.B. On Kinematic Waves I. Flood Movement in Long Rivers. Proceedings of the Royal Society of London. Series A 229 (1178), 1955, pp. 281–316.

28. Mauch, M., and Cassidy, M.J. Freeway Traffic Oscillations: Observations and Predictions. The 15th International Symposium on Transportation and Traffic flow Theory, 2002, pp. 653–673.

29. Newell, G.F. A Simplified Car-following Theory: A Lower Order Model. Transportation Research Part B, Vol. 36, No. 3, 2002, pp.195–205.

30. NGSIM. Next Generation Simulation, 2006. http://ops.fhwa.dot.gov/trafficanalysistools/ngsim.htm.

31. Ossen, S., and Hoogendoorn, S. P. Heterogeneity in Car-following Behavior: Theory and Empirics. Transportation Research Part C, Vol. 19, No. 2, 2011, pp. 182–195.

32. Peeta, S., Zhang, P., and Zhou, W. Behavior-based Analysis of Freeway Car–truck Interactions and Related Mitigation Strategies. Transportation Research Part B, Vol. 39, 2005, pp. 417-451.

33. Punzo, V., Simonelli, F. Analysis and Comparison of Microscopic Traffic Flow Models with Real Traffic Microscopic Data. Jounal of the Transportation Research Board, No. 1934, 2005, pp. 53-63.

34. Richards, P.I. Shock Waves on the Highway. Operations Research 4 (1), 1956, pp. 42–51.

35. Saifuzzaman, M., Zheng, Z. Incorporating Human-Factors in Car-Following Models: A Review of Recent Developments and Research Needs. Transportation Research Part C, Vol. 48, 2014, pp. 379-403.

36. Sen, B., Smith, J.D., and Najm, W.G. Analysis of Lane Change Crashes. Volpe National Transportation Systems Center, DOT-VNTSC NHTSA-02-03, 2002.

37. Treiber, M., Hennecke, A., and Helbing, D., Congested Traffic States in Empirical Observations and Microscopic Simulations, Physical Review E 62 (2), 2000, pp. 1805–1824.

38. Yang, C., and Regan, A., C. Impacts of Left Lane Truck Restriction on Urban Freeways. The 87nd Annual Meeting of the Transportation Research Board, 2008.

39. Yang, D., Jin, J., Ran, B., Pu, Y., and Yang, F. Modeling and Analysis of the Car-truck Heterogeneous Traffic Flow Based on Intelligent Driver Model. The 87nd Annual Meeting of the Transportation Research Board, 2013.

40. Yang, Q., and H. N. Koutsopoulos. A Microscopic Traffic Simulator for Evaluation of Dynamic Traffic Management Systems. Transportation Research, Part C, Vol. 4, No. 3, 1996, pp. 113–129.

41. Zheng, Z., Ahn, S., Chen, D., and Laval, J., Applications of Wavelet Transform for Analysis of freeway Traffic: Bottlenecks, Transient Traffic, and Traffic Oscillations. Transportation Research Part B, Vol. 45, No. 2, 2011, pp. 372–384.

This page intentionally left blank.

CFIRE

University of Wisconsin-Madison
Department of Civil and Environmental Engineering
1410 Engineering Drive, Room 270
Madison, WI 53706
Phone: 608-263-3175
Fax: 608-263-2512
cfire.wistrans.org